
Analog In-memory Training on General Non-ideal Resistive Elements: Understanding the Impact of Response Functions

Zhaoxian Wu¹ Quan Xian¹ Tayfun Gokmen² Omobayode Fagbohunbe² Tianyi Chen¹

Abstract

As the economic and environmental costs of training and deploying large vision or language models increase dramatically, analog in-memory computing (AIMC) emerges as a promising energy-efficient solution. However, the training perspective, especially its training dynamic, is underexplored. In AIMC hardware, the trainable weights are represented by the conductance of resistive elements and updated using consecutive electrical pulses. Among all the physical properties of resistive elements, the response to the pulses directly affects the training dynamics. This paper first provides a theoretical foundation for gradient-based training on AIMC hardware and studies the impact of response functions. We demonstrate that noisy update and asymmetric response functions negatively impact Analog SGD by imposing an implicit penalty term on the objective. To overcome the issue, Tiki-Taka, a residual learning algorithm, converges exactly to a critical point by optimizing a main array and a residual array bilevelly. The conclusion is supported by simulations validating our theoretical insights.

1. Introduction

The remarkable success of large vision and language models is underpinned by advances in modern hardware accelerators, such as GPU, TPU (Jouppi et al., 2023), NPU (Esmaeilzadeh et al., 2012), and NorthPole chip (Modha et al., 2023). However, the computational demands of training these models are staggering. For instance, training LLaMA (Touvron et al., 2023) cost \$2.4 million, while training GPT-3 (Brown et al., 2020) required \$4.6 million, highlighting the urgent need for more efficient computing hardware. Current mainstream hardware relies on the Von Neumann architecture, where the physical separation of memory and

processing units creates a bottleneck due to frequent and costly data movement between them.

In this context, the industry has turned its attention to *analog in-memory computing (AIMC) accelerators* based on resistive crossbar arrays (Chen, 2013; Sebastian et al., 2020; Haensch et al., 2019; Sze et al., 2017), which excel at accelerating the ubiquitous and computationally intensive matrix-vector multiplications (MVMs) operations. In AIMC hardware, the weights (matrices) are represented by the conductance states of the *resistive elements* in analog crossbar arrays (Burr et al., 2017; Yang et al., 2013), while the input and output of MVM are analog signals like voltage and current. Leveraging Kirchhoff’s and Ohm’s laws, AIMC hardware achieves $10\times$ - $10,000\times$ energy efficiency than GPU (Jain et al., 2019; Cosemans et al., 2019; Papistas et al., 2021) in the model inference.

Despite its high efficiency, *analog training* is considerably more challenging than *inference* since it involves frequent weight updates. Unlike digital hardware, where the weight increment can be applied to the original weight in the memory cell, the weights in AIMC hardware are changed by the so-called *pulse update*. When receiving electrical pulses from its peripheral circuits, the resistive elements change their conductance as a response according to the pulse polarity (Gokmen & Vlasov, 2016). However, the conductance of resistive elements increases and decreases following different response curves, leading to *asymmetric update*.

Ideally, the response to each pulse should remain unchanged regardless of time or conductance state variation, which enables concise control of the weight update. A series of works seek various resistive elements that have near-constant or at least symmetric responses. The leading candidates currently include PCM (Burr et al., 2016; Le Gallo & Sebastian, 2020), ReRAM (Jang et al., 2014; 2015; Steconci et al., 2024), ECRAM (Tang et al., 2018; Onen et al., 2022), to name a few. Currently, there is still debate regarding the most suitable resistive element for AIMC hardware. Anticipating to cover the wide ranges of resistive element candidates with various response functions, this paper studies *generic response* under a set of mild assumptions. The key concept is the *response function* of resistive elements. We are interested in how the resistive elements determine the

*Equal contribution ¹Rensselaer Polytechnic Institute, Troy, NY 12180, US ²IBM T. J. Watson Research Center, Yorktown Heights, NY 10598, US. Correspondence to: Tianyi Chen <chentianyi19@gmail.com>.

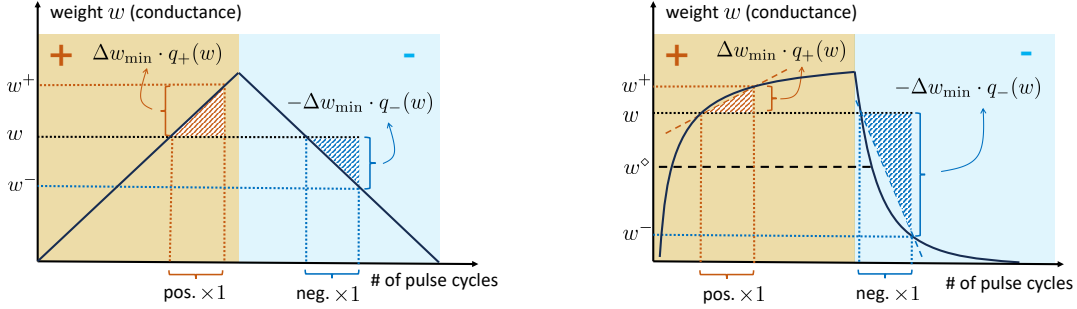


Figure 1: The weight’s response curve. Positive and negative pulses are sent continuously on the left and right half, respectively. One pulse is sent to the resistive element per cycle. Given w , the weight becomes w^+ or w^- after one positive and negative pulse, respectively. The response factors $q_+(w)$ and $q_-(w)$ are approximately the slope of the curve at w , and Δw_{\min} is the response granularity. **(Left)** Ideal response functions $q_+(w) = q_-(w)$. Every point is symmetric points. **(Right)** Asymmetric response functions $q_+(w) \neq q_-(w)$ almost everywhere expect for the symmetric point w^\diamond .

response functions and how the response functions affect the convergence properties of analog training algorithms.

1.1. Analog training and its challenges

Pulse update and asymmetric issue. In AIMC hardware, the weights of a model are stored in crossbar arrays by the conductance states of resistive elements. To modify the conductance (namely the model weights), a series of electrical pulses need to be sent to resistive elements in consecutive pulse cycles; see Figure 1. Receiving a pulse at each pulse cycle, the conductance is updated by a small amount around Δw_{\min} , which is called *response granularity*. However, resistive elements’ response varies from the positive and negative directions, reflected by different slopes in their *response curves*. The slopes, $q_+(w)$ and $q_-(w)$, is called *response functions* in this paper. All Δw_{\min} , $q_+(w)$, and $q_-(w)$ are element-dependence parameters or functions, which are set before the training process and hence kept fixed during the training. The asymmetric update leads to an asymmetric response curve and an imperfect training dynamic.

Supported by pulse update, the gradient-based training algorithms are used to optimize the weights. Consider a standard training problem with a model parameterized by $W \in \mathbb{R}^D$

$$W^* := \arg \min_{W \in \mathbb{R}^D} f(W) := \mathbb{E}_\xi[f(W; \xi)] \quad (1)$$

where $f(\cdot) : \mathbb{R}^D \rightarrow \mathbb{R}$ is the objective function and ξ is a random variable sampled from an unknown distribution.

Gradient-based training implemented by analog update.

Similar to stochastic gradient descent (SGD) in digital training (Digital SGD), the gradient-based training algorithm on AIMC hardware, Analog SGD, updates the weights by the gradient of the objective function. Let $\nabla f(W_k; \xi_k)$ be the stochastic gradient of $f(W_k; \xi_k)$ at W_k with the random variable ξ_k . The SGD updates the weight by $W_{k+1} = W_k - \alpha \nabla f(W_k; \xi_k)$ with learning rate α .

Analog SGD implements it by sending a pulse series with length about $|\Delta W|_i / \Delta w_{\min}$ to the i -th element, where $\Delta W = -\alpha \nabla f(W_k; \xi_k)$ is the *desired update*. With each pulse incurring roughly by Δw_{\min} , W_k is updated by ΔW . This process involving multiple pulse cycles to apply desired update ΔW is called Analog Update.

However, it is observed that Analog SGD suffers from a serious convergence issue due to the asymmetric update. To alleviate this issue, a family of heuristic variants, Tiki-Taka, (Gokmen & Haensch, 2020; Gokmen, 2021; Rasch et al., 2024) is proposed which introduces another crossbar array to accumulate the gradient. Recently, (Wu et al., 2024a) provides a theoretical justification for Tiki-Taka and shows that Tiki-Taka outperforms Analog SGD by eliminate the asymptotic error in Analog SGD caused by the asymmetric update. However, their work is limited to a special case of *linear response*, which are in the form of $q_+(w) = 1 - w/\tau$, $q_-(w) = 1 + w/\tau$ with hardware-specific parameter $\tau > 0$. Given more general $q_+(w)$ and $q_-(w)$, the convergence of Tiki-Taka does not trivially holds.

Challenges with generic response functions. It is not necessary for Tiki-Taka to outperform Analog SGD on generic resistive elements, even though the response functions are still linear. Consider a more generic linear response setting $q_+(w) = (1 + c_{\text{Lin}})(1 - w/\tau)$, $q_-(w) = (1 - c_{\text{Lin}})(1 + w/\tau)$ with a parameter c_{Lin} , which reduces to the setting in (Wu et al., 2024a) when $c_{\text{Lin}} = 0$. The modification is slight, but it harms the convergence of Tiki-Taka significantly.

Figure 2 shows the damage from a non-zero c_{Lin} to Tiki-Taka. Consistent with the conclusion in (Wu et al., 2024a), Tiki-Taka significantly outperforms Analog SGD when $c_{\text{Lin}} = 0$. However, when c_{Lin} is perturbed from 0.1 to 0.3, Tiki-Taka degrades dramatically and even becomes worse than Analog SGD does,

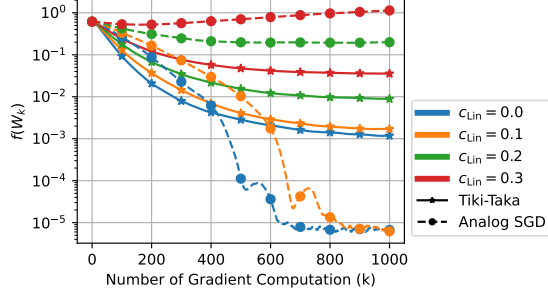


Figure 2: Objective comparison of Analog SGD and Tiki-Taka under different parameter c_{Lin} . The error plateau in the order 10^{-5} comes from the limited response granularity $\Delta w_{min} = 10^{-4}$.

indicating the non-negligible impact of the response functions. Therefore, there is no convergence guarantee for Tiki-Taka on generic responses, even with linear response. It motivates us to study the condition of the response functions for convergence.

1.2. Main results

Complementing existing empirical studies in analog in-memory computing, this paper aims to build a rigorous foundation of analog training with generic response functions. This paper builds upon the rich study of various resistive elements, including PCM, ReRAM, and so on, where the behavior of the resistive element at each pulse cycle is well studied. However, at the algorithm level, we are more interested in the dynamic of Analog Update, which describes the process of applying a desired update ΔW to the weight W implemented by sending pulse series with a proper number. Analog Update hides the details on the management of pulse series and enables us to study the convergence behavior easily. It raises a natural question:

Q1) *How do the resistive elements determine the dynamic of Analog Update?*

This paper finds that the response functions are the key to connecting pulse update and Analog Update. We start by studying the behavior of the resistive element at each pulse cycle. Based on that, we propose an approximated dynamic of Analog Update and analyze the approximation error.

The response functions are the main contributor to the difference between digital and analog training. It motivates us to study a class of benign response functions friendly to the convergence of Tiki-Taka and raises another question:

Q2) *What is the impact of generic response functions on analog training?*

To answer the question above, we establish the convergence of Analog SGD and Tiki-Taka on generic response

functions based on the proposed dynamic.

Our contributions. The contributions of the paper include:

- C1)** Building upon the equation of pulse update, we propose an approximated dynamic of Analog Update which hides non-essential details in the resistive element level while remaining mathematically tractable. Enabled by it, we study the impact of response functions directly without being limited to concrete element candidates.
- C2)** Based on critical physical properties, we focus on a class of benign response functions. Based on that, we show that analog training suffers an implicit penalty. It attracts the weights towards symmetric points and causes inexact convergence of Analog SGD.
- C3)** We demonstrate the method to alleviate the asymmetric update and implicit penalty issues by residual learning, which introduces another sequence, called *residual array*, with stationary point 0. This method leads to Tiki-Taka heuristically proposed in (Gokmen & Haensch, 2020). By properly zero-shifting so that the stationary and symmetric points overlap, Tiki-Taka provably converges to a critical point.

2. Dynamic of Non-ideal Analog Update

The primary distinction between digital and analog training is the weight update method. As discussed in Section 1, the weight update in AIMC hardware is implemented by Analog Update, which sends a series of pulses to the resistive elements. This section provides an approximated dynamic of Analog Update which focuses on the essential details in the resistive element level.

Pulse update. Consider the response of one resistive element in one cycle, which involves only one pulse. Given the initial weight w , the updated weight increases or decreases by about Δw_{min} depending on the pulse polarity, where $\Delta w_{min} > 0$ is the *response granularity* determined by elements. The granularity is further scaled by a factor, which varies by the update direction due to the *asymmetric* property of resistive elements. The notations $q_+(\cdot)$ and $q_-(\cdot)$ are used to denote the *response functions* on positive or negative sides, respectively, to describe the dominating part of the factor. In practice, the analog noise also causes a deviation of the effective factor from the response functions, referred to as *cycle variation*. It is represented by the magnitude σ_c times a random variable ξ_c with expectation 0 and variance 1. Taking all of them into account, with $s \in \{+, -\}$ being the update direction, the updated weight after receiving one pulse is $\tilde{U}_q(w, s)$ where $\tilde{U}_q(\cdot, \cdot) : \mathbb{R} \times \{+, -\} \rightarrow \mathbb{R}$ is the element-dependent update that implements the resistive element, which can be expressed as

$$\tilde{U}_q(w, s) := w + \Delta w_{min} \cdot (q_s(w) + \sigma_c \xi) \quad (2)$$

$$= \begin{cases} w + \Delta w_{\min} \cdot (q_+(w) + \sigma_c \xi_c), & s = +, \\ w - \Delta w_{\min} \cdot (q_-(w) + \sigma_c \xi_c), & s = -. \end{cases}$$

The typical signal and noise ratio $\sigma_c/q_s(w)$ is roughly 5%-100% (Gong et al., 2018; Stecconi et al., 2024), varied by the type of resistive elements. Furthermore, the response functions also vary by elements due to the imperfection in fabrication, called *element variation* (also referred to as *device variation* in literature (Gokmen & Vlasov, 2016)).

Equation (2) is a resistive element level equation. Existing work exploring the candidates of resistive elements usually reports the response curves similar to Figure 1, (Gong et al., 2022; Tang et al., 2018; Stecconi et al., 2024). Taking the difference between weights in two consecutive pulse cycles and adopting statistical approaches (Gong et al., 2018), all the element-dependent quantities, including Δw_{\min} , $q_+(\cdot)$, $q_-(\cdot)$ and σ_c , can be estimated from the response curves of the resistive elements.

Analog update implemented by pulse updates. Even though the update scheme has evolved over the years (Gokmen & Vlasov, 2016; Gokmen et al., 2017), we discuss a simplified version, called `Analog Update`, to retain the essential properties. To update the weight w by Δw , a series of pulses are sent, whose *bit length (BL)* is computed by $BL := \lceil \frac{|\Delta w|}{\Delta w_{\min}} \rceil$. After received BL pulses, the updated weight w' can be expressed as the function composition of (2) by BL times

$$w' = \underbrace{\tilde{U}_q \circ \tilde{U}_q \circ \dots \circ \tilde{U}_q}_{\times BL}(w, s) =: \tilde{U}_q^{BL}(w, s). \quad (3)$$

Roughly speaking, given an ideal response $q_+(w) = q_-(w) = 1$ and $\sigma_c = 0$, BL pulses, with Δw_{\min} increment for each individual pulse, incur the weight update Δw . Since the response granularity Δw_{\min} is scaled by the response function $q_s(w)$, the expected increment is approximately scaled by $q_s(w)$ as well. Accordingly, we propose an approximate dynamic of `Analog Update` is given by $w' \approx U_q(w, \Delta w)$, where $U_q(w, \Delta w)$ is defined by

$$U_q(w, \Delta w) := \begin{cases} w + \Delta w \cdot q_+(w), & \Delta w \geq 0, \\ w + \Delta w \cdot q_-(w), & \Delta w < 0. \end{cases} \quad (4)$$

The following theorem provides estimation of the approximation error. It has been shown empirically that the response granularity can be made sufficiently small for updating (Rao et al., 2023; Sharma et al., 2024), implying $\Delta w_{\min} \ll \Delta w$. Therefore, we establish the error estimation of the approximation based on small response granularity condition.

Theorem 2.1 (Error from discrete pulse update). *Suppose the response granularity is sufficiently small such that $\Delta w_{\min} \leq o(\Delta w)$. With the update direction $s = \text{sign}(\Delta w)$,*

the error between the true update $\tilde{U}_q^{BL}(w, s)$ and the approximated $U_q(w, \Delta w)$ is bounded by

$$\lim_{\Delta w \rightarrow 0} \frac{|\tilde{U}_q^{BL}(w, s) - U_q(w, \Delta w)|}{|\tilde{U}_q^{BL}(w, s) - w|} = 0. \quad (5)$$

The proof of Theorem 2.1 is deferred to Appendix D. In Theorem 2.1, $|\tilde{U}_q^{BL}(w, s) - U_q(w, \Delta w)|$ is the error between the true update and the proposed dynamic, while $|\tilde{U}_q^{BL}(w, s) - w|$ is the difference between original weight and the updated one. Theorem 2.1 shows that the proposed dynamic dominates the update, and the approximation error is negligible when Δw is small, which holds as Δw always includes a small learning rate in gradient-based training.

Takeaway. Theorem 2.1 enables us to discuss the impact of response functions directly without dealing with element-specific details like update granularity Δw_{\min} and cycle variation σ_c . Response functions are the bridge between the resistive element level equation (pulse update (2)) and algorithm level equation (dynamic of `Analog Update` (4)).

Compact formulations of vector. The update (4) holds at each resistive element, while the model W contains N resistive elements with different response functions $q_+(\cdot)$ and $q_-(\cdot)$. We stack all the weights w_k and expected increment Δw_k together into vectors $W_k, \Delta W_k \in \mathbb{R}^D$, where k is the iteration index¹. Similarly, the response functions $q_+(\cdot)$ and $q_-(\cdot)$ are stacked into $Q_+(\cdot)$ and $Q_-(\cdot)$, respectively. Let the notation $U_Q(W_k, \Delta W)$ on matrices W_k and ΔW denote the element-wise operation on W_k and ΔW , i.e. $[U_Q(W_k, \Delta W)]_i := U_{[Q]_i}([W_k]_i, [\Delta w]_i), \forall i \in [D]$ with $[D] := \{1, 2, \dots, D\}$ denoting the index set. The element-wise update (4) can be expressed as $W_{k+1} = U_Q(W_k, \Delta W_k)$. Leveraging the symmetric decomposition (Gokmen & Haensch, 2020; Wu et al., 2024a), we decompose $Q_-(W)$ and $Q_+(W)$ into symmetric component $F(\cdot)$ and asymmetric component $G(\cdot)$

$$F(W) := (Q_-(W) + Q_+(W))/2, \quad (6)$$

$$G(W) := (Q_-(W) - Q_+(W))/2, \quad (7)$$

which leads to a compact form of the `Analog Update`

$$W_{k+1} = W_k + \Delta W_k \odot F(W_k) - |\Delta W_k| \odot G(W_k) \quad (8)$$

where $|\cdot|$ and \odot represent the element-wise absolute value and multiplication, respectively.

¹This paper adopts w to represent the element of the weight W_k without specifying its index. The notation makes the formulations more concise and indicates that all elements are updated in parallel.

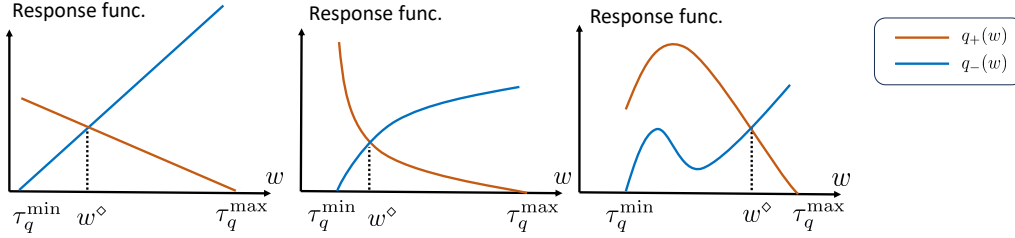


Figure 3: Examples of response functions from Definition 2.2; w^\diamond is the symmetric point.

Gradient-based training algorithms on AIMC hardware.

In (8), the desired update ΔW_k varies based on different algorithms. Replacing ΔW_k with the stochastic gradient $\nabla f(W_k; \xi_k)$, we obtain the dynamic of Analog SGD as

$$W_{k+1} = W_k - \alpha \nabla f(W_k; \xi_k) \odot F(W_k) - \alpha |\nabla f(W_k; \xi_k)| \odot G(W_k) \quad (9)$$

where $\alpha > 0$ is the learning rate and ξ_k is the noise introduced at time k . The noise can come from both data sampling and analog noise, like thermal or shot noise.

Saturation. To avoid reaching arbitrarily high or low conductance states, resistive elements get *saturated* when they keep receiving the same pulses. Constrained by that, the conductance of the resistive element with $q_+(\cdot)$ and $q_-(\cdot)$ is bounded by a *dynamic range* $[\tau^{\min}, \tau^{\max}]$ where τ^{\min} and τ^{\max} are the saturation points with zero responses, i.e. $q_+(\tau^{\max}) = q_-(\tau^{\min}) = 0$. Near the saturation points, the asymmetric issue is significant, and thus, the update in one direction is suppressed, considerably impacting the convergence. On the contrary, if a point w^\diamond satisfies $q_-(w^\diamond) = q_+(w^\diamond)$, the analog update behaves like a digital update. We refer to w^\diamond as *symmetric point*. Symmetric points are typically located in the interior of the dynamic range and are far from saturation.

Stacking all w^\diamond into a vector $W^\diamond \in \mathbb{R}$. Observe that the function $G(W)$ is large near the saturation points while almost zero around W^\diamond , implying it can reflect the degree of saturation. At the same time, $F(W)$ is the average of the response functions in two directions. As we will see in Sections 3.2 and 4, the ratios $\frac{G(W)}{\sqrt{F(W)}}$ plays a critical role in the convergence behaviors.

Response function class. Since the behavior of resistive elements is always governed by physical laws, we are interested in a class of response functions that reflect some physical properties. First, the conductance ends up increasing when receiving a positive pulse and vice versa, leading to positive response functions. On top of that, we also assume the response functions are differentiable (and hence continuous) for mathematical tractability. Taking them and conductance saturation into account, we are interested in the following response function class.

Definition 2.2 (Response function class). $q_+(\cdot)$ and $q_-(\cdot)$

with dynamic range $[\tau^{\min}, \tau^{\max}]$ satisfy

- **(Positive-definiteness)** $q_+(w) > 0, \forall w < \tau^{\max}$ and $q_-(w) > 0, \forall w > \tau^{\min}$;
- **(Differentiable)** $q_+(\cdot)$ and $q_-(\cdot)$ are differentiable;
- **(Saturation)** $q_+(\tau^{\max}) = q_-(\tau^{\min}) = 0$.

Definition 2.2 covers a wide range of response functions. Figure 3 showcases three examples from the response functions class, including linear, non-linear monotonic, and even non-monotonic functions.

3. Implicit Penalty and Inexact Convergence of Analog SGD

As a critical impact from the response functions, an implicit penalty term is applied to the objective, leading to an asymptotic error in Analog SGD.

3.1. Implicit penalty

We first give an intuition through a situation where W_k is already a critical point, i.e., $\mathbb{E}_\xi[\nabla f(W_k; \xi)] = 0$. Recall that stochastic gradient descent on digital hardware (Digital SGD) is stable in expectation, i.e.

$$\mathbb{E}_{\xi_k}[W_{k+1}] = W_k - \mathbb{E}_{\xi_k}[\alpha \nabla f(W_k; \xi_k)] = W_k. \quad (10)$$

However, this does not work for Analog SGD

$$\begin{aligned} \mathbb{E}_{\xi_k}[W_{k+1}] &= W_k - \mathbb{E}_{\xi_k}[\alpha \nabla f(W_k; \xi_k) \odot F(W_k) \\ &\quad - \alpha |\nabla f(W_k; \xi_k)| \odot G(W_k)] \\ &= W_k - \alpha \mathbb{E}_{\xi_k}[|\nabla f(W_k; \xi_k)| \odot G(W_k)] \neq W_k. \end{aligned} \quad (11)$$

Consider a simplified version that the weight is a scalar ($D = 1$) and the function $G(W)$ is strictly monotonically decreasing² to help us gain intuition on the impact of the drift in (11). Recall $G(W^\diamond) = 0$ at the symmetric point W^\diamond . $G(W) > 0$ when $W > W^\diamond$ and $G(W) < 0$ otherwise. Consequently, (11) indicates that $\mathbb{E}_{\xi_k}[W_{k+1}] < W_k$ when $W_k > W^\diamond$ and $\mathbb{E}_{\xi_k}[W_{k+1}] > W_k$ otherwise. Consequently, W_k suffers from a drift tendency towards W^\diamond . In addition, it can be speculated that the penalty coefficient supposes to be

²It happens when both $q_+(\cdot)$ and $q_-(\cdot)$ are strictly monotonic.

proportional to the noise level since the drift is proportional to $\mathbb{E}_{\xi_k}[|\nabla f(W_k; \xi_k)|]$, which is the first moment of noise $\mathbb{E}_{\xi_k}[|\nabla f(W_k; \xi_k) - \mathbb{E}_{\xi}[\nabla f(W_k; \xi)]|]$ in essence.

The following theorem formalizes the implicit penalty effect. Before that, we define an accumulated asymmetric function $R_c(\cdot) : \mathbb{R}^D \rightarrow \mathbb{R}^D$, whose gradient is $R(W) := \frac{G(W)}{F(W)}$, i.e. $\nabla R_c(W) = R(W) = \frac{G(W)}{F(W)}$. Consequently, if $R(W)$ is strictly monotonic, $R_c(W)$ reaches its minimum at the symmetric point W^\diamond where $R(W^\diamond) = 0$ so that it penalizes the weight away symmetric point.

Theorem 3.1 (Implicit penalty, short version). *Suppose $\mathbb{E}_{\xi_k}[|\nabla f(W_k; \xi_k) - \mathbb{E}_{\xi}[\nabla f(W_k; \xi)]|]$ is a constant $\Sigma \in \mathbb{R}^D$ and let $D = 1$. Analog SGD implicitly optimizes the following penalized objective*

$$\min_W f_\Sigma(W) := f(W) + \langle \Sigma, R_c(W) \rangle. \quad (12)$$

The full version of Theorem 3.1 and its proof are deferred to Appendix E. In Theorem 3.1, $R_c(W)$ plays the role of penalty to force the weight toward a symmetric point. As shown in Appendix E, $R_c(W)$ has a simple expression on linear response functions when $c_{\text{Lin}} = 0$, leading (12) to

$$\min_W f_\Sigma(W) := f(W) + \frac{\Sigma}{2\tau} \|W\|^2 \quad (13)$$

which has the objective with ℓ_2 regularization. In addition, the implicit penalty has a coefficient proportional to the noise level Σ and inversely proportional to the dynamic range τ . It implies that the implicit penalty becomes active only when gradients are noisy, and it is amplified when the noise is large.

Implicit penalty. When the gradient is noisy, an implicit penalty attracts Analog SGD toward symmetric points.

3.2. Inexact Convergence of Analog SGD

Due to the implicit penalty, Analog SGD only converges to a critical point inexactly. Before showing that, We introduce a series of assumptions on the objective, as well as noise.

Assumption 3.2 (Objective). The objective $f(W)$ is L -smooth and is lower bounded by f^*

Assumption 3.3 (Unbiasness and bounded variance). The sample $\{\xi_k : k \in [K]\}$ are independently and identically sampled from a distribution over times $k \in [K]$. Furthermore, the stochastic gradient is unbiased and has bounded variance, i.e., $\mathbb{E}_{\xi_k}[\nabla f(W_k; \xi_k)] = \nabla f(W_k)$ and $\mathbb{E}_{\xi_k}[\|\nabla f(W_k; \xi_k) - \nabla f(W_k)\|^2] \leq \sigma^2$.

Assumption 3.2–3.3 are standard in non-convex optimization (Bottou et al., 2018; Wu et al., 2024a). Additionally,

similar to the setting in (Wu et al., 2024a), we also assume that the saturation degree is bounded, given by a lower bound of response functions.

Assumption 3.4 (Bounded saturation). There exists a constant $H_{\min} > 0$ such that $\min\{Q_+(W) \odot Q_-(W)\} > H_{\min}$.

Assumption 3.4 requires that W_k remains far from saturation points, which is a mild assumption in actual training. This paper considers the average gradient square norm as the convergence metric, given by $E_K := \frac{1}{K} \sum_{k=0}^{K-1} \|\nabla f(W_k)\|^2$. Now, we establish the convergence of Analog SGD.

Theorem 3.5 (Inexact convergence of Analog SGD). *Under Assumption 3.2–3.4, if the learning rate is set as $\alpha = O(1/\sqrt{K})$, it holds that*

$$E_K \leq O\left(\sqrt{\sigma^2/K} + \sigma^2 S_K^{\text{ASGD}}\right) \quad (14)$$

where S_K^{ASGD} denotes the amplification factor given by

$$S_K^{\text{ASGD}} := \frac{1}{K} \sum_{k=0}^{K-1} \left\| \frac{G(W_k)}{\sqrt{F(W_k)}} \right\|_\infty^2.$$

The proof of Theorem 3.5 is deferred to Appendix F. Theorem 3.5 suggests that the convergence metric E_K is upper bounded by two terms: the first term vanishes at a rate of $O(\sqrt{\sigma^2/K})$, which matches the Digital SGD’s convergence rate (Bottou et al., 2018) up to a constant; the second term contributes to the asymptotic error of Analog SGD, which does not vanish with the number of iterations K .

Impact of saturation/asymmetric update. The exact expression of S_K^{ASGD} depends on the specific noise distribution and thus is difficult to reach. However, S_K^{ASGD} reflects the saturation degree near the critical point W^* when W_k converges to a neighborhood of W^* . If W^* is far from the symmetric point W^\diamond , S_K^{ASGD} becomes large, leading to a large E_K^{ASGD} and a large asymptotic error. In contrast, if W^* remains close to the symmetric point W^\diamond , the asymptotic error is small.

4. Mitigating Implicit Penalty by Residual Learning: Tiki-Taka

The asymptotic error in Analog SGD is a fundamental issue that arises from the mismatch between the symmetric point and the critical point. An idealistic remedy for the inexact convergence is carefully shifting the weights to ensure the stationary point is close to a symmetric point. However, determining the appropriate adjustment is always challenging, as the critical point is difficult to pinpoint before the actual training. Therefore, an ideal solution to address this issue is to jointly construct a sequence with a predictable stationary point and a proper shift of the symmetric point.

Residual learning. Our solution overlaps the algorithmic stationary point and physical symmetric point on the special

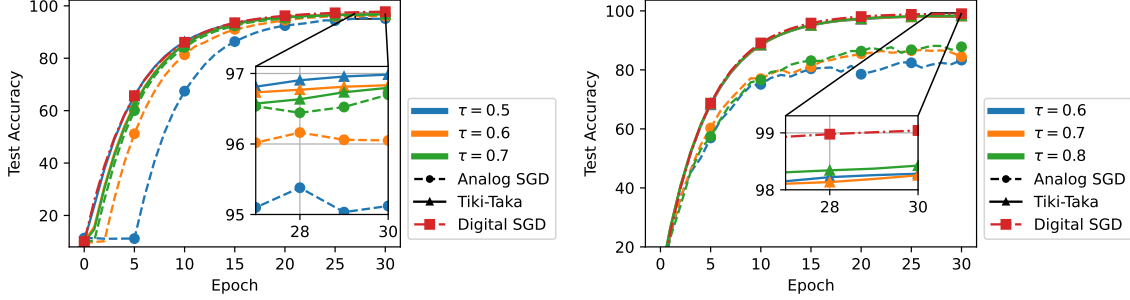


Figure 4: The test accuracy curves for the model training on MNIST dataset under different τ ; **(Left)** FCN. **(Right)** CNN.

point 0. Besides the main analog array, W_k , we maintain another array, P_k , whose stationary point is 0. A natural choice is the *residual* of the weight given by the solution of the following problem

$$P^*(W) \in \arg \min_{P \in \mathbb{R}^D} f(W + \gamma P) \quad (15)$$

where $\gamma \geq 0$ is a mixing coefficient. Noticing that 0 is a solution of (15) if W is already a solution of (1). Furthermore, the gradient of $f(W + \gamma P)$ with respect to P , given by $\nabla_P f(W + \gamma P) = \gamma \nabla f(W + \gamma P)$, is accessible with fair expense, enabling us to introduce a sequence P_k to track the residual of W_k by optimizing (15)

$$P_{k+1} = P_k - \alpha \nabla f(\bar{W}_k; \xi_k) \odot F(P_k) - \alpha |\nabla f(\bar{W}_k; \xi_k)| \odot G(P_k). \quad (16)$$

Ideally, it holds that $P_k \approx P^*(W_k)$ after (16), and hence it can be expected that $f(W_k + \gamma P_k) \leq f(W_k)$ so that one step of transfer leads to descent on $f(W_k)$

$$W_{k+1} = W_k + \beta P_{k+1} \odot F(W_k) - \beta |P_{k+1}| \odot G(W_k) \quad (17)$$

which solves the following problem by approximating the gradient $P^*(W)$ by P_k

$$\arg \min_{W \in \mathbb{R}^D} \|P^*(W)\|^2. \quad (18)$$

The updates (16) and (17) are performed alternatively until convergence³. By solving a bilevel optimization problem (15) and (18) approximately, our solution recovers the update of Tiki-Taka (Gokmen & Haensch, 2020).

On the response functions side, it is naturally required to let zero be a symmetric point, i.e. $G(0) = 0$, which can be implemented by zero-shifting technique (Kim et al., 2019) by subtracting a reference array.

Convergence properties of Tiki-Taka. We begin by analyzing the convergence of Tiki-Taka without considering the zero-shift first, enabling us to understand how the zero-shift response function benefit the convergence.

³In principle, $F(\cdot)$ and $G(\cdot)$ vary from W_k and P_k . We adopt the same notations for them just for convenience.

If the optimal point W^* exists and is unique, the solution of (15) has a closed form $P^*(W) := \frac{W^* - W}{\gamma}$. At that time, the objective of (18) is equivalent to $\|W^* - W\|^2$. However, the solutions of (15) and (18) are non-unique in general, especially for non-convex objectives with multiple local minima. To ensure the existence and uniqueness of W^* , we assume the objective is strongly convex.

Assumption 4.1 (μ -strong convexity). The objective $f(W)$ is μ -strongly convex.

Under the strongly convex assumption, the optimal point W^* is unique. We believe the requirement of strong convexity is non-essence, and the proof can be extended to more general cases, which is left for future work.

Involving two sequences W_k and P_k , Tiki-Taka converges in different senses, including: (a) the residual array P_k converges to the optimal point $P^*(W_k)$ of (15); (b) W_k converges to the critical point of (18) or the optimal point W^* ; (c) the sum $\bar{W}_k = W_k + \gamma P_k$ converges to a critical point where $\nabla f(\bar{W}_k)$. Taking all these into account, we define the convergence metric as

$$E_K^{TT} := \frac{1}{K} \sum_{k=0}^{K-1} \mathbb{E} \left[\|\nabla f(\bar{W}_k)\|^2 + O(\|P_k - P^*(W_k)\|^2) + O(\|W_k - W^*\|^2) \right]. \quad (19)$$

For simplicity, the constants in front of some terms in E_K^{TT} are hidden. Now, we provide the convergence of Tiki-Taka with generic responses.

Theorem 4.2 (Convergence of Tiki-Taka). *Under Assumptions 3.2–3.4, and 4.1, with learning rate $\alpha = O(\sqrt{1/\sigma^2 K})$, $\beta = O(\alpha \gamma^{3/2})$, it holds for Tiki-Taka that*

$$E_K^{TT} \leq O\left(\sqrt{\sigma^2/K} + \sigma^2 S_K^{TT}\right) \quad (20)$$

where S_K^{TT} denotes the amplification factor of P_k given by

$$S_K^{TT} := \frac{1}{K} \sum_{k=0}^{K-1} \left\| \frac{G(P_k)}{\sqrt{F(P_k)}} \right\|_{\infty}^2.$$

The proof of Theorem 4.2 is deferred to Appendix G. Theorem 4.2 claims that Tiki-Taka converges at the rate

	CIFAR10			CIFAR100		
	DSGD	ASGD	TT	DSGD	ASGD	TT
ResNet18	95.43±0.13	84.47±3.40	94.81±0.09	81.12±0.25	68.98±1.01	76.17±0.23
ResNet34	96.48±0.02	95.43±0.12	96.29±0.12	83.86±0.12	78.98±0.55	80.58±0.11
ResNet50	96.57±0.10	94.36±1.16	96.34±0.04	83.98±0.11	79.88±1.26	80.80±0.22

Table 1: Analog training with the *power response* for fine-tuning task on CIFAR10/100 using models from ResNet family. The test accuracy is reported. DSGD, ASGD, and TT represent Digital SGD, Analog SGD, Tiki-Taka, respectively.

$O\left(\sqrt{\sigma^2/K}\right)$ to a neighbor of critical point with radius $O(\sigma^2 S_K^{TT})$, which share almost the same expression with the convergence of Analog SGD. The difference lies in the amplification factor S_K^{TT} and S_K^{ASGD} , where the former depends on P_k while the latter depends on W_k .

Impact of response functions. Response function affects the Analog SGD and Tiki-Taka similarly. However, attributed to the residual array, constructing response functions to enable exact convergence of Tiki-Taka is feasible.

As we have discussed, P_k tends to $P^*(W_k)$ which tends to 0 given W_k tends to W^* . Resistive elements with response functions such that $G(P) = 0$ when $P = 0$ is required for the exact convergence.

Assumption 4.3. (Zero-shifted symmetric point) $P = 0$ is a symmetric point, i.e. $G(0) = 0$.

Under it and the Lipschitz continuity of the response functions, it holds directly that $\left\|\frac{G(P_k)}{\sqrt{F(P_k)}}\right\|_\infty \leq L_S \|P_k\|_\infty$ for a constant $L_S \geq 0$. Consequently, when $P_k \rightarrow P^*(W_k) \rightarrow 0$ as $W_k \rightarrow W^*$, the asymptotic error disappears. Formally, the following corollary holds true.

Corollary 4.4 (Exact convergence of Tiki-Taka). *Under Assumption 4.3 and the conditions in Theorem 4.2, if $\gamma \geq \Omega(H_{\min}^{-1/5})$, it holds that $E_K^{TT} \leq O\left(\sqrt{\sigma^2 L/K}\right)$.*

The proof of Corollary 4.4 is deferred to Appendix G.5. Corollary 4.4 demonstrates the failure of Tiki-Taka in Figure 2. The symmetric point is $w^\diamond = c_{\text{Lin}}\tau$ in this example, which violates Assumption 4.3 when $c_{\text{Lin}} \neq 0$ and hence introduces asymptotic error into Tiki-Taka.

5. Numerical Simulations

In this section, we verify the main theoretical results by simulations on both synthetic datasets and real datasets. We use the open source toolkit IBM Analog Hardware Acceleration Kit (AIHWKIT) (Rasch et al., 2021) to simulate the behaviors of Analog SGD and Tiki-Taka. Each simulation is repeated three times, and the mean and standard deviation are reported. More details can be referred to in Appendix I.

We consider two types of response functions in our simulations: power and exponential response functions with dynamic ranges $[-\tau, \tau]$, while the symmetric point is 0, as required by Corollary 4.4.

MNIST FCN/CNN. We train fully-connected network (FCN) and convolution neural network (CNN) on the MNIST dataset and compare the performance of Analog SGD and Tiki-Taka under various τ on power responses; see the results in Figure 4. By tracking residual, Tiki-Taka outperforms Analog SGD and reaches comparable accuracy with Digital SGD. For both architectures, the accuracy of Tiki-Taka drops by $< 1\%$. In contrast, Analog SGD takes a few epochs to achieve observable accuracy increment in FCN training, rendering a slower convergence rate than Tiki-Taka. In CNN training, Analog SGD’s accuracy increases more slowly than Tiki-Taka does and finally gets stuck at about 80%. It is consistent with the theoretical claims.

CIFAR10/CIFAR100 ResNet. We fine-tune three models from the ResNet family with different scales on CIFAR10/CIFAR100 datasets. The power response functions with the parameter $\gamma_{\text{res}} = 3.0$ and $\tau = 0.1$ are used, whose results are shown in Table 1. The results show that the Tiki-Taka outperforms Analog SGD by about 1.0% in most of the cases in ResNet34/50, and the gap even reaches about 10.0% for ResNet18 training on the CIFAR100 dataset.

6. Conclusions and Limitations

This paper studies the impact of response functions on gradient-based training in analog in-memory computing hardware. We first formulate the dynamic of Analog Update based on the pulse update rule, which is a bridge between the equation at the resistive element level and the one at the algorithm level. Based on this dynamic, we study the convergence of two gradient-based analog training algorithms, Analog SGD and Tiki-Taka. The theoretical results demonstrate that Analog SGD converges to a critical point inexactly with asymptotic error, which comes from the noise and asymmetric update. To overcome this issue, Tiki-Taka introduces a residual array whose stationary point is 0. By properly shifting the sym-

metric point of the residual array, Tiki-Taka provably converges to a critical point exactly. Numerical simulations verify the claims about the implicit bias and the efficacy of Tiki-Taka against Analog SGD.

References

- Bottou, L., Curtis, F. E., and Nocedal, J. Optimization methods for large-scale machine learning. *SIAM review*, 60(2):223–311, 2018.
- Brown, T., Mann, B., Ryder, N., Subbiah, M., Kaplan, J. D., Dhariwal, P., Neelakantan, A., Shyam, P., Sastry, G., Askell, A., et al. Language models are few-shot learners. *Advances in neural information processing systems*, 33: 1877–1901, 2020.
- Burr, G. W., BrightSky, M. J., Sebastian, A., Cheng, H.-Y., Wu, J.-Y., Kim, S., Sosa, N. E., Papandreou, N., Lung, H.-L., Pozidis, H., Eleftheriou, E., and Lam, C. H. Recent Progress in Phase-Change Memory Technology. *IEEE Journal on Emerging and Selected Topics in Circuits and Systems*, 6(2):146–162, 2016. ISSN 2156-3357.
- Burr, G. W., Shelby, R. M., Sebastian, A., Kim, S., Kim, S., Sidler, S., Virwani, K., Ishii, M., Narayanan, P., Fumarola, A., et al. Neuromorphic computing using non-volatile memory. *Advances in Physics: X*, 2(1):89–124, 2017.
- Chen, A. A comprehensive crossbar array model with solutions for line resistance and nonlinear device characteristics. *IEEE Transactions on Electron Devices*, 60(4): 1318–1326, 2013.
- Cosemans, S., Verhoef, B.-E., Doevenspeck, J., Papistas, I. A., Cathoor, F., Debacker, P., Mallik, A., and Verkest, D. Towards 10000TOPS/W DNN inference with analog in-memory computing – a circuit blueprint, device options and requirements. In *IEEE International Electron Devices Meeting*, pp. 22.2.1–22.2.4, 2019.
- Ernault, M., Grollier, J., Querlioz, D., Bengio, Y., and Scellier, B. Equilibrium propagation with continual weight updates. *arXiv preprint arXiv:2005.04168*, 2020.
- Esmailzadeh, H., Sampson, A., Ceze, L., and Burger, D. Neural acceleration for general-purpose approximate programs. In *IEEE/ACM international symposium on microarchitecture*, pp. 449–460. IEEE, 2012.
- Fuller, E. J., Keene, S. T., Melianas, A., Wang, Z., Agarwal, S., Li, Y., Tuchman, Y., James, C. D., Marinella, M. J., Yang, J. J., Salleo, A., and Talin, A. A. Parallel programming of an ionic floating-gate memory array for scalable neuromorphic computing. *Science*, 364(6440):570–574, 2019.
- Gokmen, T. Enabling training of neural networks on noisy hardware. *Frontiers in Artificial Intelligence*, 4:1–14, 2021.
- Gokmen, T. and Haensch, W. Algorithm for training neural networks on resistive device arrays. *Frontiers in Neuroscience*, 14, 2020.
- Gokmen, T. and Vlasov, Y. Acceleration of deep neural network training with resistive cross-point devices: Design considerations. *Frontiers in neuroscience*, 10:333, 2016.
- Gokmen, T., Onen, M., and Haensch, W. Training deep convolutional neural networks with resistive cross-point devices. *Frontiers in neuroscience*, 11:538, 2017.
- Gong, N., Idé, T., Kim, S., Boybat, I., Sebastian, A., Narayanan, V., and Ando, T. Signal and noise extraction from analog memory elements for neuromorphic computing. *Nature communications*, 9(1):2102, 2018.
- Gong, N., Rasch, M., Seo, S.-C., Gasasira, A., Solomon, P., Bragaglia, V., Consiglio, S., Higuchi, H., Park, C., Brew, K., et al. Deep learning acceleration in 14nm CMOS compatible ReRAM array: device, material and algorithm co-optimization. In *IEEE International Electron Devices Meeting*, 2022.
- Guo, R., Lin, W., Yan, X., Venkatesan, T., and Chen, J. Ferroic tunnel junctions and their application in neuromorphic networks. *Applied physics reviews*, 7(1), 2020.
- Haensch, W., Gokmen, T., and Puri, R. The next generation of deep learning hardware: Analog computing. *Proceedings of the IEEE*, 107(1):108–122, 2019.
- Hughes, T. W., Williamson, I. A., Minkov, M., and Fan, S. Wave physics as an analog recurrent neural network. *Science advances*, 5(12):eaay6946, 2019.
- Jain, S. et al. Neural network accelerator design with resistive crossbars: Opportunities and challenges. *IBM Journal of Research and Development*, 63(6):10–1, 2019.
- Jang, J.-W., Park, S., Jeong, Y.-H., and Hwang, H. ReRAM-based synaptic device for neuromorphic computing. In *IEEE International Symposium on Circuits and Systems*, pp. 1054–1057, 2014.
- Jang, J.-W., Park, S., Burr, G. W., Hwang, H., and Jeong, Y.-H. Optimization of conductance change in $\text{Pr}_{1-x}\text{Ca}_x\text{MnO}_3$ -based synaptic devices for neuromorphic systems. *IEEE Electron Device Letters*, 36(5):457–459, 2015.
- Jouppi, N., Kurian, G., Li, S., Ma, P., Nagarajan, R., Nai, L., Patil, N., Subramanian, S., Swing, A., Towles, B., et al. TPU v4: An optically reconfigurable supercomputer for machine learning with hardware support for embeddings. In *Annual International Symposium on Computer Architecture*, pp. 1–14, 2023.

- Jung, S., Lee, H., Myung, S., Kim, H., Yoon, S. K., Kwon, S.-W., Ju, Y., Kim, M., Yi, W., Han, S., et al. A crossbar array of magnetoresistive memory devices for in-memory computing. *Nature*, 601(7892):211–216, 2022.
- Kendall, J., Pantone, R., Manickavasagam, K., Bengio, Y., and Scellier, B. Training end-to-end analog neural networks with equilibrium propagation. *arXiv preprint arXiv:2006.01981*, 2020.
- Kim, H., Rasch, M. J., Gokmen, T., Ando, T., Miyazoe, H., Kim, J.-J., Rozen, J., and Kim, S. Zero-shifting technique for deep neural network training on resistive cross-point arrays. *arXiv preprint arXiv:1907.10228*, 2019.
- Le Gallo, M. and Sebastian, A. An overview of phase-change memory device physics. *Journal of Physics D: Applied Physics*, 53(21):213002, 2020.
- Lim, S., Kwak, M., and Hwang, H. Improved synaptic behavior of CBRAM using internal voltage divider for neuromorphic systems. *IEEE Transactions on Electron Devices*, 65(9):3976–3981, 2018.
- Merrikh-Bayat, F., Guo, X., Klachko, M., Prezioso, M., Likharev, K. K., and Strukov, D. B. High-performance mixed-signal neurocomputing with nanoscale floating-gate memory cell arrays. *IEEE Transactions on Neural Networks and Learning Systems*, 29(10):4782–4790, 2017.
- Modha, D. S., Akopyan, F., Andreopoulos, A., Appuswamy, R., Arthur, J. V., Cassidy, A. S., Datta, P., DeBole, M. V., Esser, S. K., Otero, C. O., et al. Neural inference at the frontier of energy, space, and time. *Science*, 382(6668):329–335, 2023.
- Momeni, A., Rahmani, B., Scellier, B., Wright, L. G., McMahan, Peter L and Wanjura, C. C., Li, Y., Skalli, A., Berloff, N. G., Onodera, T., Oguz, I., Morichetti, F., del Hougne, P., Le Gallo, M., Sebastian, A., Mirhoseini, A., Zhang, C., Marković, D., Brunner, D., Moser, C., Gigan, S., Marquardt, F., Ozcan, A., Grollier, J., Liu, A. J., Psaltis, D., Alù, A., and Fleury, R. Training of physical neural networks. *arXiv preprint arXiv:2406.03372*, 2024.
- Nandakumar, S. R., Le Gallo, M., Boybat, I., Rajendran, B., Sebastian, A., and Eleftheriou, E. Mixed-precision architecture based on computational memory for training deep neural networks. In *IEEE International Symposium on Circuits and Systems*, pp. 1–5, 2018.
- Nandakumar, S. R., Le Gallo, M., Piveteau, C., Joshi, V., Mariani, G., Boybat, I., Karunaratne, G., Khaddam-Aljameh, R., Egger, U., Petropoulos, A., Antonakopoulos, T., Rajendran, B., Sebastian, A., and Eleftheriou, E. Mixed-precision deep learning based on computational memory. *Frontiers in Neuroscience*, 14, 2020.
- Nesterov, Y. *Introductory Lectures on Convex Optimization: A Basic Course*. Springer, 2013.
- Onen, M., Emond, N., Wang, B., Zhang, D., Ross, F. M., Li, J., Yildiz, B., and Del Alamo, J. A. Nanosecond protonic programmable resistors for analog deep learning. *Science*, 377(6605):539–543, 2022.
- Papistas, I. A., Cosemans, S., Rooseleer, B., Doevenspeck, J., Na, M.-H., Mallik, A., Debacker, P., and Verkest, D. A 22 nm, 1540 TOP/s/W, 12.1 TOP/s/mm² in-memory analog matrix-vector-multiplier for DNN acceleration. In *IEEE Custom Integrated Circuits Conference*, pp. 1–2. IEEE, 2021.
- Psaltis, D., Brady, D., Gu, X.-G., and Lin, S. Holography in artificial neural networks. *Nature*, 343(6256):325–330, 1990.
- Rao, M., Tang, H., Wu, J., Song, W., Zhang, M., Yin, W., Zhuo, Y., Kiani, F., Chen, B., Jiang, X., et al. Thousands of conductance levels in memristors integrated on CMOS. *Nature*, 615(7954):823–829, 2023.
- Rasch, M. J., Moreda, D., Gokmen, T., Le Gallo, M., Carta, F., Goldberg, C., El Maghraoui, K., Sebastian, A., and Narayanan, V. A flexible and fast PyTorch toolkit for simulating training and inference on analog crossbar arrays. *IEEE International Conference on Artificial Intelligence Circuits and Systems*, pp. 1–4, 2021.
- Rasch, M. J., Carta, F., Fagbohunge, O., and Gokmen, T. Fast and robust analog in-memory deep neural network training. *Nature Communications*, 15(1):7133–7147, 2024.
- Scellier, B. and Bengio, Y. Equilibrium propagation: Bridging the gap between energy-based models and backpropagation. *Frontiers in computational neuroscience*, 11:24, 2017.
- Scellier, B., Ernoult, M., Kendall, J., and Kumar, S. Energy-based learning algorithms for analog computing: a comparative study. *Advances in Neural Information Processing Systems*, 36, 2024.
- Sebastian, A., Le Gallo, M., Khaddam-Aljameh, R., and Eleftheriou, E. Memory devices and applications for in-memory computing. *Nature Nanotechnology*, 15:529–544, 2020.
- Sharma, D., Rath, S. P., Kundu, B., Korkmaz, A., Thompson, D., Bhat, N., Goswami, S., Williams, R. S., and Goswami, S. Linear symmetric self-selecting 14-bit kinetic molecular memristors. *Nature*, 633(8030):560–566, 2024.

- Stecconi, T., Bragaglia, V., Rasch, M. J., Carta, F., Horst, F., Falcone, D. F., Ten Kate, S. C., Gong, N., Ando, T., Olziersky, A., et al. Analog resistive switching devices for training deep neural networks with the novel Tiki-Taka algorithm. *Nano Letters*, 24(3):866–872, 2024.
- Sze, V., Chen, Y.-H., Yang, T.-J., and Emer, J. S. Efficient processing of deep neural networks: A tutorial and survey. *Proceedings of the IEEE*, 105(12):2295–2329, 2017.
- Tait, A. N., De Lima, T. F., Zhou, E., Wu, A. X., Nahmias, M. A., Shastri, B. J., and Prucnal, P. R. Neuromorphic photonic networks using silicon photonic weight banks. *Scientific reports*, 7(1):7430, 2017.
- Tang, J., Bishop, D., Kim, S., Copel, M., Gokmen, T., Todorov, T., Shin, S., Lee, K.-T., Solomon, P., Chan, K., et al. ECRAM as scalable synaptic cell for high-speed, low-power neuromorphic computing. In *IEEE International Electron Devices Meeting*, pp. 13–1. IEEE, 2018.
- Touvron, H., Lavril, T., Izacard, G., Martinet, X., Lachaux, M.-A., Lacroix, T., Rozière, B., Goyal, N., Hambro, E., Azhar, F., et al. Llama: Open and efficient foundation language models. *arXiv preprint arXiv:2302.13971*, 2023.
- Wang, P., Xu, F., Wang, B., Gao, B., Wu, H., Qian, H., and Yu, S. Three-dimensional NAND flash for vector-matrix multiplication. *IEEE Transactions on Very Large Scale Integration Systems*, 27(4):988–991, 2018a.
- Wang, Z., Joshi, S., Savel’Ev, S., Song, W., Midya, R., Li, Y., Rao, M., Yan, P., Asapu, S., Zhuo, Y., et al. Fully memristive neural networks for pattern classification with unsupervised learning. *Nature Electronics*, 1(2):137–145, 2018b.
- Watfa, M., Garcia-Ortiz, A., and Sassatelli, G. Energy-based analog neural network framework. *Frontiers in Computational Neuroscience*, 17:1114651, 2023.
- Wright, L. G., Onodera, T., Stein, M. M., Wang, T., Schachter, D. T., Hu, Z., and McMahon, P. L. Deep physical neural networks trained with backpropagation. *Nature*, 601(7894):549–555, 2022.
- Wu, Z., Gokmen, T., Rasch, M. J., and Chen, T. Towards exact gradient-based training on analog in-memory computing. 2024a.
- Wu, Z., Xiao, Q., Gokmen, T., Tsai, H., Maghraoui, K. E., and Chen, T. Pipeline gradient-based model training on analog in-memory accelerators. *arXiv preprint arXiv:2410.15155*, 2024b.
- Xiang, Y., Huang, P., Han, R., Li, C., Wang, K., Liu, X., and Kang, J. Efficient and robust spike-driven deep convolutional neural networks based on NOR flash computing array. *IEEE Transactions on Electron Devices*, 67(6):2329–2335, 2020.
- Xiao, Z., Naik, V. B., Lim, J. H., Hou, Y., Wang, Z., and Shao, Q. Adapting magnetoresistive memory devices for accurate and on-chip-training-free in-memory computing. *Science Advances*, 10(38):eadp3710, 2024.
- Yang, J. J., Strukov, D. B., and Stewart, D. R. Memristive devices for computing. *Nature nanotechnology*, 8(1):13, 2013.

Appendix for “Analog In-memory Training on Non-ideal Resistive Elements: Understanding the Impact of Response Functions”

Table of Contents

A Literature Review	12
B Relation with the result in (Wu et al., 2024a)	14
C Useful Lemmas and Proofs	15
C.1 Lemma C.1: Properties of weighted norm	15
C.2 Lemma C.2: Properties of weighted norm	15
C.3 Lemma C.3: Lipschitz continuity of analog update	15
C.4 Lemma C.4: Element-wise product error	16
D Proof of Theorem 2.1: Error from Pulse Update	16
E Proof of Theorem 3.1: Implicit Bias of Analog Training	17
F Proof of Theorem 3.5: Convergence of Analog SGD	19
G Proof of Theorem 4.2: Convergence of Tiki-Taka	22
G.1 Main proof	22
G.2 Proof of Lemma G.1: Descent of sequence \bar{W}_k	26
G.3 Proof of Lemma G.2: Descent of sequence W_k	29
G.4 Proof of Lemma G.3: Descent of sequence P_k	31
G.5 Proof of Corollary 4.4: Exact convergence of Tiki-Taka	33
H Proof of Theorem H.1: Convergence of Analog GD	34
I Simulation Details and Additional Results	36
I.1 Power and Exponential Response Functions	36
I.2 Least squares problem	36
I.3 Classification problem	37
I.4 Additional performance on real datasets	38
I.5 Ablation study on cycle variation	38
I.6 Ablation study on various response functions	39
I.7 Ablation study on γ	39

A. Literature Review

This section briefly reviews literature that is related to this paper, as complementary to Section 1.

Resistive element. A series of works seek various resistive elements that have near-constant or at least symmetric responses. The leading candidates currently include PCM (Burr et al., 2016; Le Gallo & Sebastian, 2020), ReRAM (Jang et al., 2014; 2015; Stecconi et al., 2024), CBRAM (Lim et al., 2018; Fuller et al., 2019), ECRAM (Tang et al., 2018; Onen et al., 2022), MRAM (Jung et al., 2022; Xiao et al., 2024), FTJ (Guo et al., 2020) or flash memory (Wang et al., 2018a; Xiang et al., 2020; Merrih-Bayat et al., 2017).

However, the resistive element possessing symmetric updates may not be the best option in terms of manufacturing. For example, although ECRAM provides almost symmetric updates, it is still less competitive than ReRAM as ReRAM has a

faster response speed and lower pulse voltage (Stecconi et al., 2024). The suitability of the resistive elements is evaluated based on metrics across multiple dimensions, such as the number of conductance states, retention, material endurance, switching energy, response speed, manufacturing cost, and cell size. Among them, this paper is only interested in the impact of response functions in the training.

Gradient-based training on AIMC hardware. A series of works focuses on implementing back-propagation (BP) and gradient-based training on AIMC hardware. The seminal work (Gokmen & Vlasov, 2016; Gokmen et al., 2017) leverages the rank-one structure of the gradient and implements Analog SGD by a stochastic pulse update scheme, *rank-update*. Rank-update significantly accelerates the gradient descent step by avoiding dealing the gradients with $O(N^2)$ elements directly but using two $O(N)$ vectors for update instead, where N is the numbers of matrix row and column. To alleviate the *asymmetric update issue*, researchers also design various of Analog SGD variants, Tiki-Taka algorithm family (Gokmen & Haensch, 2020; Gokmen, 2021; Rasch et al., 2024). The key components of Tiki-Taka are introducing a *residual array* to stabilize the training. Apart from the rank-update, a hybrid scheme that performs forward and backward in the analog domain but computes the gradients in the digital domain has been proposed in (Nandakumar et al., 2018; 2020). Their solution, referred to as *mixed-precision update*, provides a more accurate gradient signal but requires $5\times-10\times$ higher overhead compared to the rank-update scheme (Rasch et al., 2024).

Attributed to these efforts, analog training has empirically shown great promise in achieving a similar level of accuracy as digital training on chip prototype, with reduced energy consumption and training time (Wang et al., 2018b; Gong et al., 2022). Simultaneously, the parallel acceleration solution with AIMC hardware is also under exploration (Wu et al., 2024b). Despite its good performance, it is still mysterious about when and why they work.

Theoretical foundation of gradient-based training. The closely related result comes from the convergence study of Tiki-Taka (Wu et al., 2024a). Similar to our work, they attempt to model the dynamic and provide the convergence properties of Analog SGD and Tiki-Taka. However, their work is limited to a special linear response function. Furthermore, their paper considers a simplified version of Tiki-Taka, with a hyper-parameter $\gamma = 0$ (see Section 4). As we will show empirically and theoretically, Tiki-Taka benefits from a non-zero γ . Consequently, We compare the results briefly in Table 2 and comprehensively in Appendix B.

	γ	Generic response	Linear response
Tiki-Taka (Wu et al., 2024a)	$= 0$	\times	$O\left(\sqrt{\frac{1}{K} \frac{1}{1-33P_{\max}^2/\tau^2}}\right)$
Tiki-Taka [Corollary 4.4]	$\neq 0$	$O\left(\sqrt{\frac{1}{K} \frac{1}{H_{\min}^{\text{TT}}}}\right)$	$O\left(\sqrt{\frac{1}{K} \frac{1}{1-P_{\max}^2/\tau^2}}\right)$

Table 2: Comparison between our paper and (Wu et al., 2024a). Mixing-coefficient γ is a hyper-parameter of Tiki-Taka. ‘‘Generic response’’ and ‘‘Linear response’’ columns are the convergence rates in the corresponding settings. K represents the number of iterations. H_{\min}^{TT} and $P_{\max}^2/\tau^2 < 1$ measure the saturation while the former one reduces to the latter on linear response functions.

Energy-based models and equilibrium propagation. Apart from achieving explicit gradient signals by the BP, there are also attempts to train models based on *equilibrium propagation* (EP, (Scellier & Bengio, 2017)), which provides a biologically plausible alternative to traditional BP. EP is applicable to a series of energy-based models, where the forward pass is performed by minimizing an energy function (Wafra et al., 2023; Scellier et al., 2024). The update signal in EP is computed by measuring the output difference between a free phase and an active phase. EP eliminates the need for BP non-local weight transport mechanism, making it more compatible with neuromorphic and energy-efficient hardware (Kendall et al., 2020; Ernoult et al., 2020). We highlight here that the approach to attain update signals (BP or EP) is orthogonal to the update mechanism (pulse update). Their difference lies in the objective $f(W_k)$, which is hidden in this paper. Therefore, building upon the pulse update, our work is applicable to both BP and EP.

Physical neural network. The model executing on AIMC hardware, which leverages resistive crossbar array to accelerate MVM operation, is a concrete implementation of physical neural networks (PNNs, (Wright et al., 2022; Momeni et al., 2024)). PNN is a generic concept of implementing neural networks via a physical system in which a set of tunable parameters, such as holographic grating (Psaltis et al., 1990), wave-based systems (Hughes et al., 2019), and photonic networks (Tait et al., 2017). Our work particularly focuses on training with AIMC hardware, but the methodology developed in this paper can be transferred to the study of other PNNs.

B. Relation with the result in (Wu et al., 2024a)

Similar to this paper, (Wu et al., 2024a) also attempts to model the dynamic of analog training. They shows that Analog SGD converges to a critical point of problem (1) inexactly with an asymptotic error, and Tiki-Taka converges to a critical point exactly. In this section, we compare our results with our results and theirs.

As discussed in Section 1, (Wu et al., 2024a) studies the analog training on special linear response functions

$$q_+(w) = 1 - \frac{w}{\tau}, \quad q_-(w) = 1 + \frac{w}{\tau}. \quad (21)$$

It can be checked that the symmetric point is 0 while the dynamic range of it is $[-\tau, \tau]$. The symmetric and asymmetric components is defined by $F(W) = 1$ and $G(W) = \frac{W}{\tau}$, respectively. It indicates $F_{\max} = 1$. Furthermore, they assume the bounded weight saturation by assuming bounded weights, i.e., $\|W_k\|_{\infty} \leq W_{\max}, \forall k \in [K]$ with a constant $W_{\max} < \tau$. Under this assumption, the lower bounds of response functions are given by

$$\min\{H(W_k)\} = \min\{Q_+(W_k) \odot Q_-(W_k)\} = 1 - \left(\frac{\|W_k\|_{\infty}}{\tau}\right)^2 \quad (22)$$

$$H_{\min}^{\text{ASGD}} = \min\{H(W_k)\} = 1 - \left(\frac{W_{\max}}{\tau}\right)^2. \quad (23)$$

Convergence of Analog SGD. As we will show in Remark F.1 at the end of Appendix F, inequality (14) can be improved when the saturation never happens

$$\frac{1}{K} \sum_{k=0}^{K-1} \mathbb{E}[\|\nabla f(W_k)\|^2] \quad (24)$$

$$\leq \frac{4F_{\max}^2}{H_{\min}^{\text{TT}}} \sqrt{\frac{(f(W_0) - f^*)\sigma^2 L}{K}} + 2F_{\max}\sigma^2 \times \frac{1}{K} \sum_{k=0}^{K-1} \left\| \frac{G(W_k)}{\sqrt{F(W_k)}} \right\|_{\infty}^2 / \min\{H(W_k)\} \quad (25)$$

$$\leq O\left(\sqrt{\frac{(f(W_0) - f^*)\sigma^2 L}{K}} \frac{1}{1 - W_{\max}^2/\tau^2}\right) + 2\sigma^2 \times \frac{1}{K} \sum_{k=0}^{K-1} \frac{\|W_k\|_{\infty}^2/\tau^2}{1 - \|W_k\|_{\infty}^2/\tau^2}$$

which is exactly the result in (Wu et al., 2024a).

Convergence of Tiki-Taka. It is shown that a non-zero γ in (16) improves the training accuracy (Gokmen & Haensch, 2020). However, (Wu et al., 2024a) considers a special case with $\gamma = 0$ while this paper considers a non-zero γ . As we will discuss latter in this section, different γ leads to different convergence behaviors of Tiki-Taka.

With the linear response, if we also assume the bounded saturation of P_k by letting $\|P_k\|_{\infty} \leq P_{\max}$, the minimal average response function is given by $H_{\min}^{\text{TT}} = 1 - \left(\frac{P_{\max}}{\tau}\right)^2$. The upper bound in Corollary 4.4 becomes

$$\frac{1}{K} \sum_{k=0}^{K-1} \|\nabla f(\bar{W}_k)\|^2 \leq O\left(\frac{1}{1 - P_{\max}^2/\tau^2} \sqrt{\frac{(f(W_0) - f^*)\sigma^2 L}{K}}\right). \quad (26)$$

As a comparison, without introducing a non-zero γ , (Wu et al., 2024a) shows that convergence rate of Tiki-Taka is only

$$\frac{1}{K} \sum_{k=0}^{K-1} \|\nabla f(W_k)\|^2 \leq O\left(\frac{1}{1 - 33P_{\max}^2/\tau^2} \sqrt{\frac{(f(W_0) - f^*)\sigma^2 L}{K}}\right). \quad (27)$$

Even though it is not a completely fair comparison since two paper relies on different assumptions, it is still worthy to compare the analysis in two paper. (Wu et al., 2024a) assumes the noise should be non-zero, i.e. $[\mathbb{E}_{\xi}[\|\nabla f(W; \xi)\|]]_i \geq c_{\text{noise}}\sigma, \forall i \in [D]$ holds for a non-zero constant c_{noise} . Instead, this paper does not make this assumption but assumes that the objective is strongly convex. As mentioned in Section 4, the strong convexity is introduced only to ensure the existence

of $P^*(W_k)$. Therefore, we believe it can be relaxed, and the convergence rate can remain unchanged, which is left as a future work. Taking that into account, we believe the comparison can provide insight of how the non-zero γ improves the convergence rate of Tiki-Taka.

Why does non-zero γ improve the convergence rate of Tiki-Taka? As discussed in Section 4, P_k is interpreted as a residual array that optimizes (15). In the ideal setting that $F(W) = 1$ and $G(W) = 0$, it can be shown that P_k converges to $P^*(W_k)$ if W_k is fixed and P_k is kept updated, even though the $W_k \neq W^*$ (hence $\nabla f(W_k) \neq 0$).

Instead, without a non-zero γ , (Wu et al., 2024a) points out that P_k is an approximation of clear gradient by showing

$$\begin{aligned} & \mathbb{E}_{\xi_k} [\|P_{k+1} - C\nabla f(W_k)\|^2] \\ & \leq \left(1 - \frac{\beta}{C}\right) \|P_k - C\nabla f(W_k)\|^2 + O(\beta C') \|\nabla f(W_k)\|^2 + \text{remainder} \end{aligned} \quad (28)$$

where C, C' are constants depending on the resistive element and model dimension, and the ‘‘remainder’’ is the non-essential terms. Consider the case that W_k is fixed and (16) is kept iterating, in which case the increment on P_k is constant since $\gamma = 0$. Telescoping (28) we find the upper bound above only guarantee that

$$\limsup_{k \rightarrow \infty} \mathbb{E} [\|P_{k+1} - C\nabla f(W_k)\|^2] \leq O(CC' \|\nabla f(W_k)\|^2) \quad (29)$$

which means that P_k tracks the gradient accurately only when $\nabla f(W_k)$ reaches zero asymptotically. Consequently, the less accurate approximation leads to a slower rate than this paper.

C. Useful Lemmas and Proofs

C.1. Lemma C.1: Properties of weighted norm

Lemma C.1. $\|W\|_S$ has the following properties: (a) $\|W\|_S = \|W \odot \sqrt{S}\|$; (b) $\|W\|_S \leq \|W\| \sqrt{\|S\|_\infty}$; (c) $\|W\|_S \geq \|W\| \sqrt{\min\{S\}}$.

Proof of Lemma C.1. The lemma can be proven easily by definition. \square

C.2. Lemma C.2: Properties of weighted norm

A direct property from Definition 2.2 is that all $q_+(\cdot)$, $q_-(\cdot)$, and $F(\cdot)$ are bounded, as guaranteed by the following lemma.

Lemma C.2. The following statements are valid for all $W \in \mathcal{R}$. (a) $F(\cdot)$ is element-wise upper bounded by a constant $F_{\max} > 0$, i.e., $\|F(W)\|_\infty \leq F_{\max}$; (b) $Q_+(\cdot)$ and $\nabla Q_-(\cdot)$ are element-wise bounded by L_Q , i.e., $\|\nabla Q_+(W)\|_\infty \leq L_Q$, $\|\nabla Q_-(W)\|_\infty \leq L_Q$.

C.3. Lemma C.3: Lipschitz continuity of analog update

Lemma C.3. The increment defined in (8) is Lipschitz continuous with respect to ΔW under any weighted norm $\|\cdot\|_S$, i.e., for any $W, \Delta W, \Delta W' \in \mathbb{R}^D$ and $S \in \mathbb{R}_+^D$, it holds

$$\begin{aligned} & \|\Delta W \odot F(W) - |\Delta W| \odot G(W) - (\Delta W' \odot F(W) - |\Delta W'| \odot G(W))\|_S \\ & \leq F_{\max} \|\Delta W - \Delta W'\|_S. \end{aligned} \quad (30)$$

Proof of Lemma C.3. We prove for the case where $D = 1$ and $S = 1$, and the general case can be proven similarly. Notice that the absolute value $|\cdot|$ and vector norm $\|\cdot\|$, scalar multiplication \times and element-wise multiplication \odot , are equivalent at that situation. We adopt both notations just for readability.

$$\begin{aligned} & \|\Delta W \odot F(W) - |\Delta W| \odot G(W) - (\Delta W' \odot F(W) - |\Delta W'| \odot G(W))\| \\ & = \|(\Delta W - \Delta W') \odot F(W) - (|\Delta W| - |\Delta W'|) \odot G(W)\|. \end{aligned} \quad (31)$$

Since $\|\Delta W - \Delta W'\| \geq \||\Delta W| - |\Delta W'|\|$ and $|G(W)| \leq |F(W)|$, we have

$$\|(\Delta W - \Delta W') \odot F(W) - (|\Delta W| - |\Delta W'|) \odot G(W)\| \quad (32)$$

$$\begin{aligned}
 &\leq |(\Delta W - \Delta W') \odot (F(W) - |G(W)|)| \\
 &\leq |\Delta W - \Delta W'| |F(W) - |G(W)|| \\
 &\leq F_{\max} |\Delta W - \Delta W'|
 \end{aligned}$$

which completes the proof. \square

C.4. Lemma C.4: Element-wise product error

Lemma C.4. Let $U, V, Q \in \mathbb{R}^D$ be vectors indexed by $[D]$. Then the following inequality holds

$$\langle U, V \odot Q \rangle \geq C_+ \langle U, V \rangle - C_- \langle |U|, |V| \rangle \quad (33)$$

where the constant C_+ and C_- are defined by

$$C_+ := \frac{1}{2} (\max\{Q\} + \min\{Q\}), \quad (34)$$

$$C_- := \frac{1}{2} (\max\{Q\} - \min\{Q\}). \quad (35)$$

Proof of Lemma C.4. For any vectors $U, V, Q \in \mathbb{R}^D$, it is always valid that

$$\begin{aligned}
 \langle U, V \odot Q \rangle &= \sum_{i \in [D]} [U]_i [V]_i [Q]_i \quad (36) \\
 &= \sum_{i \in [D], [U]_i [V]_i \geq 0} [U]_i [V]_i [Q]_i + \sum_{i \in [D], [U]_i [V]_i < 0} [U]_i [V]_i [Q]_i \\
 &\geq \min\{Q\} \times \left(\sum_{i \in [D], [U]_i [V]_i \geq 0} [U]_i [V]_i \right) + \max\{Q\} \times \left(\sum_{i \in [D], [U]_i [V]_i < 0} [U]_i [V]_i \right) \\
 &\stackrel{(a)}{=} C_+ \left(\sum_{i \in [D], [U]_i [V]_i \geq 0} [U]_i [V]_i \right) - C_- \left(\sum_{i \in [D], [U]_i [V]_i \geq 0} |[U]_i [V]_i| \right) \\
 &\quad + C_+ \left(\sum_{i \in [D], [U]_i [V]_i < 0} [U]_i [V]_i \right) - C_- \left(\sum_{i \in [D], [U]_i [V]_i < 0} |[U]_i [V]_i| \right) \\
 &= C_+ \sum_{i \in [D]} [U]_i [V]_i - C_- \sum_{i \in [D]} |[U]_i [V]_i| \\
 &= C_+ \langle U, V \rangle - C_- \langle |U|, |V| \rangle
 \end{aligned}$$

where (a) uses the following equality

$$\min\{Q\} [U]_i [V]_i = C_+ [U]_i [V]_i - C_- |[U]_i [V]_i|, \quad \text{if } [U]_i [V]_i \geq 0, \quad (37)$$

$$\max\{Q\} [U]_i [V]_i = C_+ [U]_i [V]_i - C_- |[U]_i [V]_i|, \quad \text{if } [U]_i [V]_i < 0. \quad (38)$$

This completes the proof. \square

D. Proof of Theorem 2.1: Error from Pulse Update

Theorem 2.1 (Error from discrete pulse update). Suppose the response granularity is sufficiently small such that $\Delta w_{\min} \leq o(\Delta w)$. With the update direction $s = \text{sign}(\Delta w)$, the error between the true update $\tilde{U}_q^{\text{BL}}(w, s)$ and the approximated $U_q(w, \Delta w)$ is bounded by

$$\lim_{\Delta w \rightarrow 0} \frac{|\tilde{U}_q^{\text{BL}}(w, s) - U_q(w, \Delta w)|}{|\tilde{U}_q^{\text{BL}}(w, s) - w|} = 0. \quad (5)$$

Proof of Theorem 2.1. Recall the definition of the bit length is

$$\text{BL} := \left\lceil \frac{|\Delta w|}{\Delta w_{\min}} \right\rceil = \Theta \left(\frac{|\Delta w|}{\Delta w_{\min}} \right) \quad (39)$$

leading to

$$|\text{BL} \Delta w_{\min} - |\Delta w|| \leq \Delta w_{\min} \quad \text{or} \quad |s \text{BL} \Delta w_{\min} - \Delta w| \leq \Delta w_{\min}. \quad (40)$$

Notice that the update responding to each pulse is a $\Theta(\Delta w_{\min})$ term. Directly manipulating $U_p^{\text{BL}}(w, s)$ and expanding it in Taylor series to the first-order term yields

$$\begin{aligned} U_p^{\text{BL}}(w, s) &= w + s \cdot \Delta w_{\min} \sum_{t=0}^{\text{BL}-1} q_s(w + \Theta(t \Delta w_{\min})) + \Delta w_{\min} \sum_{t=0}^{\text{BL}-1} \sigma_c \xi_t \\ &= w + s \cdot \Delta w_{\min} \sum_{t=0}^{\text{BL}-1} q_s(w) + \sum_{t=0}^{\text{BL}-1} \Theta(t (\Delta w_{\min})^2) + \Delta w_{\min} \sum_{t=0}^{\text{BL}-1} \sigma_c \xi_t \\ &= w + s \cdot \Delta w_{\min} \cdot \text{BL} \cdot q_s(w) + \Theta(\text{BL}^2 (\Delta w_{\min})^2) + \Delta w_{\min} \cdot \sqrt{\text{BL}} \cdot \sigma_c \xi \\ &= w + \Delta w \cdot q_s(w) + (s \text{BL} \Delta w_{\min} - \Delta w) + \Theta((\Delta w)^2) + \sqrt{\Delta w_{\min}} \cdot \sqrt{\Delta w} \cdot \sigma_c \xi \\ &= U_q(w, \Delta w) + \Theta(\Delta w_{\min}) + \Theta((\Delta w)^2) + \Theta(\sqrt{\Delta w_{\min}} \cdot \sqrt{\Delta w} \cdot \sigma_c) \end{aligned} \quad (41)$$

where $\xi := \frac{1}{\sqrt{\text{BL}}} \sum_{t=0}^{\text{BL}-1} \xi_t$ is the accumulated noise with variance 1. The proof is completed. \square

E. Proof of Theorem 3.1: Implicit Bias of Analog Training

In this section, we provide a full version of Theorem 3.1. Before that, we formally define the accumulated asymmetric function $R_c(W) : \mathbb{R}^D \rightarrow \mathbb{R}^D$ element-wise. Let $R(W) := \frac{G(W)}{F(W)}$ be the asymmetric ratio and $R_c(W)$ is defined by

$$[R_c(W)]_i := \int_{\tau_i^{\min}}^{[W]_i} [R(W)]_i d[W]_i \quad (42)$$

which satisfies

$$\nabla R_c(W) = R(W) \quad \text{and} \quad \nabla \langle \Sigma, R_c(W) \rangle = \Sigma \odot R(W). \quad (43)$$

Since we do not further assume stronger properties for response functions, like monotonicity, it is hard to provide strong claims on the shape of $R(W)$ or $R_c(W)$. Here we provide the expression of $R_c(W)$ for the linear response functions $Q_+(W) = 1 - \frac{W}{\tau}$, $Q_-(W) = 1 + \frac{W}{\tau}$. In this case, $F(W) = 1$ and $G(W) = \frac{W}{\tau}$ based on definition (6); and hence $R(W) = \frac{G(W)}{F(W)} = \frac{W}{\tau}$. Accordingly, the accumulated asymmetric function is given by

$$\begin{aligned} [R_c(W)]_i &= \int_{\tau_i^{\min}}^{[W]_i} [R(W)]_i d[W]_i = \int_{\tau_i^{\min}}^{[W]_i} \frac{[W]_i}{\tau} d[W]_i \\ &= \frac{1}{2\tau} ([W]_i)^2 - \frac{1}{2\tau} (\tau_i^{\min})^2. \end{aligned} \quad (44)$$

Therefore, the last term in the objective (12) becomes

$$\begin{aligned} \langle \Sigma, R_c(W) \rangle &= \sum_{i=1}^D [\Sigma]_i [R_c(W)]_i = \sum_{i=1}^D [\Sigma]_i \left(\frac{1}{2\tau} ([W]_i)^2 - \frac{1}{2\tau} (\tau_i^{\min})^2 \right) \\ &= \frac{1}{2\tau} \|W\|_{\Sigma}^2 + \text{const.} \end{aligned} \quad (45)$$

which is a weighted ℓ_2 norm regularization term. It reduces to (13) in the scalar case.

If the ratio $R(W)$ is monotonic at each coordinate, $R_c(W)$ reaches its minimum at W^{\diamond} .

Theorem E.1 (Implicit Penalty, full version of Theorem 3.1). *Let $T(w)$ denote the effective update of Analog SGD.*

$$T(W) := \left| \frac{\mathbb{E}_\xi [U_q(W, -\alpha f'(W; \xi))] - W}{\alpha} \right| = |\mathbb{E}_\xi [f'(w; \xi)] \odot F(W) - \mathbb{E}_\xi [|f'(W; \xi)|] \odot G(W)|. \quad (46)$$

Analog SGD implicitly optimizes the following penalized objective

$$\min_W f_\Sigma(W) := f(W) + \langle \Sigma, R_c(W) \rangle \quad (47)$$

in the sense that there exists a point W^S given by

$$W^S := (\nabla^2 f(W^*) - \nabla R(W^\diamond)\Sigma)^{-1}(\nabla^2 f(W^*) W^* - \nabla R(W^\diamond)\Sigma W^\diamond) \quad (48)$$

such that $\|\nabla f_\Sigma(W^S)\| \leq O((W^\diamond - W^*)^2)$ and $T(W^S) \leq O((W^\diamond - W^*)^2)$. Both $T(W^S)$ and $\|\nabla f_\Sigma(W^S)\|$ are significantly smaller than $T(W^\diamond) = O(|W^\diamond - W^*|)$ and $T(W^*) = O(|W^\diamond - W^*|)$ when W^\diamond is close to W^* .

If W is a scalar, i.e. $D = 1$, (48) reduces to (13)

$$\min_W f_\Sigma(W) := f(W) + \frac{\Sigma}{2\tau} \|W\|^2 \quad (49)$$

with its solution

$$W^S := \frac{f''(W^*) W^* - R'(W^\diamond)\Sigma W^\diamond}{f''(W^*) - R'(W^\diamond)\Sigma}. \quad (50)$$

Proof of Theorem 3.1 and E.1. We separately show that $\|\nabla f_\Sigma(W)\| \leq O((W^\diamond - W^*)^2)$ and $T(W^S) \leq O((W^\diamond - W^*)^2)$.

Proof of $\|\nabla f_\Sigma(W)\| \leq O((W^\diamond - W^*)^2)$. The gradient of the penalized objective $f_\Sigma(W)$ is given by

$$\nabla f_\Sigma(W) = \nabla f(W) + \Sigma \odot R(W). \quad (51)$$

Leveraging the fact that $\nabla f(W^*) = 0$, $\frac{G(W^\diamond)}{F(W^\diamond)} = 0$, as well as Taylor expansion given by

$$\nabla f(W^S) = \nabla f(W^*) + \nabla^2 f(W^*)(W^S - W^*) + O((W^S - W^*)^2), \quad (52)$$

$$\frac{G(W^S)}{F(W^S)} = \frac{G(W^\diamond)}{F(W^\diamond)} + \nabla R(W^\diamond)(W^S - W^\diamond) + O((W^S - W^\diamond)^2), \quad (53)$$

we bound the gradient of the penalized objective as follows

$$\begin{aligned} \|\nabla f_\Sigma(W)\| &= \left\| \nabla f(W^S) - \Sigma \odot \frac{G(W^S)}{F(W^S)} \right\| \\ &= \left\| \nabla^2 f(W^*)(W^S - W^*) + O((W^S - W^*)^2) - \Sigma \odot (\nabla R(W^\diamond)(W^S - W^\diamond)) + O((W^S - W^\diamond)^2) \right\| \\ &= O((W^S - W^*)^2) + O((W^S - W^\diamond)^2) \\ &= O((W^* - W^\diamond)^2) \end{aligned} \quad (54)$$

where the last inequality holds by the definition of W^S .

Proof of $T(w^S) \leq O((w^\diamond - w^*)^2)$. By the definition of effective update $T(W^S)$, we have

$$\begin{aligned} &\left\| \frac{\mathbb{E}_\xi [U_q(W^S, -\alpha \nabla f(W^S; \xi))] - W^S}{\alpha} \right\| \\ &= \left\| \mathbb{E}_\xi [\nabla f(W^S; \xi)] \odot F(W^S) - \mathbb{E}_\xi [|\nabla f(W^S; \xi)|] \odot G(W^S) \right\| \\ &\leq \left\| \left(\nabla f(W^S) - \mathbb{E}_\xi [|\nabla f(W^S; \xi)|] \odot \frac{G(W^S)}{F(W^S)} \right) \right\| F_{\max} \end{aligned} \quad (55)$$

$$\begin{aligned}
 &\leq \left\| \nabla f(W^S) - \mathbb{E}_\xi[\nabla f(W^S; \xi) - \nabla f(W^S)] \odot \frac{G(W^S)}{F(W^S)} \right\| F_{\max} \\
 &\quad + \left\| (\mathbb{E}_\xi[\nabla f(W^S; \xi)] - \mathbb{E}_\xi[\nabla f(W^S; \xi) - \nabla f(W^S)]) \odot \frac{G(W^S)}{F(W^S)} \right\| F_{\max} \\
 &\leq \|\nabla f_\Sigma(W)\| F_{\max} + \left\| (\mathbb{E}_\xi[\nabla f(W^S; \xi)] - \mathbb{E}_\xi[\nabla f(W^S; \xi) - \nabla f(W^S)]) \odot \frac{G(W^S)}{F(W^S)} \right\| F_{\max}
 \end{aligned}$$

The first term in the right-hand side (RHS) of (55) is already bounded by (54). By inequality $\|x\| - \|y\| \leq \|x - y\|$ for any $x, y \in \mathbb{R}$, the second term in the RHS of (55) is bounded by

$$\begin{aligned}
 &\left\| (\mathbb{E}_\xi[\nabla f(W^S; \xi)] - \mathbb{E}_\xi[\nabla f(W^S; \xi) - \nabla f(W^S)]) \odot \frac{G(W^S)}{F(W^S)} \right\| \\
 &\leq \left\| |\nabla f(W^S)| \odot \frac{G(W^S)}{F(W^S)} \right\| \\
 &= \left\| |\nabla f(W^S) - \nabla f(W^*)| \odot \left(\frac{G(W^S)}{F(W^S)} - \frac{G(W^\diamond)}{F(W^\diamond)} \right) \right\| \\
 &\leq O(|W^S - W^*|) \cdot O(|W^S - W^\diamond|) \\
 &= O((W^* - W^\diamond)^2)
 \end{aligned} \tag{56}$$

Plugging back (54) and (56) into (55) shows $T(w^S) \leq O((w^\diamond - w^*)^2)$. It is trivial to prove $T(W^\diamond) = O(|W^\diamond - W^*|)$ and $T(W^*) = O(|W^\diamond - W^*|)$ by the definition of W^S and (52). \square

F. Proof of Theorem 3.5: Convergence of Analog SGD

Theorem 3.5 (Inexact convergence of Analog SGD). *Under Assumption 3.2–3.4, if the learning rate is set as $\alpha = O(1/\sqrt{K})$, it holds that*

$$E_K \leq O\left(\sqrt{\sigma^2/K} + \sigma^2 S_K^{\text{ASGD}}\right) \tag{14}$$

where S_K^{ASGD} denotes the amplification factor given by $S_K^{\text{ASGD}} := \frac{1}{K} \sum_{k=0}^{K-1} \left\| \frac{G(W_k)}{\sqrt{F(W_k)}} \right\|_\infty^2$.

Proof of Theorem 3.5. The L -smooth assumption (Assumption 3.2) implies that

$$\mathbb{E}_{\xi_k}[f(W_{k+1})] \leq f(W_k) + \underbrace{\mathbb{E}_{\xi_k}[\langle \nabla f(W_k), W_{k+1} - W_k \rangle]}_{(a)} + \underbrace{\frac{L}{2} \mathbb{E}_{\xi_k}[\|W_{k+1} - W_k\|^2]}_{(b)}. \tag{57}$$

Next, we will handle the second and the third terms in the RHS of (57) separately.

Bound of the second term (a). To bound term (a) in the RHS of (57), we leverage the assumption that noise has expectation 0 (Assumption 3.3)

$$\begin{aligned}
 &\mathbb{E}_{\xi_k}[\langle \nabla f(W_k), W_{k+1} - W_k \rangle] \\
 &= \alpha \mathbb{E}_{\xi_k} \left[\left\langle \nabla f(W_k) \odot \sqrt{F(W_k)}, \frac{W_{k+1} - W_k}{\alpha \sqrt{F(W_k)}} + (\nabla f(W_k; \xi_k) - \nabla f(W_k)) \odot \sqrt{F(W_k)} \right\rangle \right] \\
 &= -\frac{\alpha}{2} \|\nabla f(W_k) \odot \sqrt{F(W_k)}\|^2 \\
 &\quad - \frac{1}{2\alpha} \mathbb{E}_{\xi_k} \left[\left\| \frac{W_{k+1} - W_k}{\sqrt{F(W_k)}} + \alpha (\nabla f(W_k; \xi_k) - \nabla f(W_k)) \odot \sqrt{F(W_k)} \right\|^2 \right] \\
 &\quad + \frac{1}{2\alpha} \mathbb{E}_{\xi_k} \left[\left\| \frac{W_{k+1} - W_k}{\sqrt{F(W_k)}} + \alpha \nabla f(W_k; \xi_k) \odot \sqrt{F(W_k)} \right\|^2 \right].
 \end{aligned} \tag{58}$$

The second term of the RHS of (58) is bounded by

$$\begin{aligned}
 & \frac{1}{2\alpha} \mathbb{E}_{\xi_k} \left[\left\| \frac{W_{k+1} - W_k}{\sqrt{F(W_k)}} + \alpha(\nabla f(W_k; \xi_k) - \nabla f(W_k)) \odot \sqrt{F(W_k)} \right\|^2 \right] \\
 &= \frac{1}{2\alpha} \mathbb{E}_{\xi_k} \left[\left\| \frac{W_{k+1} - W_k + \alpha(\nabla f(W_k; \xi_k) - \nabla f(W_k)) \odot F(W_k)}{\sqrt{F(W_k)}} \right\|^2 \right] \\
 &\geq \frac{1}{2\alpha F_{\max}} \mathbb{E}_{\xi_k} [\|W_{k+1} - W_k + \alpha(\nabla f(W_k; \xi_k) - \nabla f(W_k)) \odot F(W_k)\|^2].
 \end{aligned} \tag{59}$$

The third term in the RHS of (58) can be bounded by variance decomposition and bounded variance assumption (Assumption 3.3)

$$\begin{aligned}
 & \frac{1}{2\alpha} \mathbb{E}_{\xi_k} \left[\left\| \frac{W_{k+1} - W_k}{\sqrt{F(W_k)}} + \alpha \nabla f(W_k; \xi_k) \odot \sqrt{F(W_k)} \right\|^2 \right] \\
 &= \frac{\alpha}{2} \mathbb{E}_{\xi_k} \left[\left\| |\nabla f(W_k; \xi_k)| \odot \frac{G(W_k)}{\sqrt{F(W_k)}} \right\|^2 \right] \\
 &\leq \frac{\alpha}{2} \left\| |\nabla f(W_k)| \odot \frac{G(W_k)}{\sqrt{F(W_k)}} \right\|^2 + \frac{\alpha\sigma^2}{2} \left\| \frac{G(W_k)}{\sqrt{F(W_k)}} \right\|_{\infty}^2.
 \end{aligned} \tag{60}$$

Define the saturation vector $H(W_k) \in \mathbb{R}^D$ by

$$\begin{aligned}
 H(W_k) &:= F(W_k)^{\odot 2} - G(W_k)^{\odot 2} = (F(W_k) + G(W_k)) \odot (F(W_k) - G(W_k)) \\
 &= Q_+(W_k) \odot Q_-(W_k).
 \end{aligned} \tag{61}$$

Note that the first term in the RHS of (58) and the second term in the RHS of (60) can be bounded by

$$\begin{aligned}
 & -\frac{\alpha}{2} \|\nabla f(W_k) \odot \sqrt{F(W_k)}\|^2 + \frac{\alpha}{2} \left\| |\nabla f(W_k)| \odot \frac{G(W_k)}{\sqrt{F(W_k)}} \right\|^2 \\
 &= -\frac{\alpha}{2} \sum_{d \in [D]} \left([\nabla f(W_k)]_d^2 \left([F(W_k)]_d - \frac{[G(W_k)]_d^2}{[F(W_k)]_d} \right) \right) \\
 &= -\frac{\alpha}{2} \sum_{d \in [D]} \left([\nabla f(W_k)]_d^2 \left(\frac{[F(W_k)]_d^2 - [G(W_k)]_d^2}{[F(W_k)]_d} \right) \right) \\
 &\leq -\frac{\alpha}{2F_{\max}} \sum_{d \in [D]} ([\nabla f(W_k)]_d^2 ([F(W_k)]_d^2 - [G(W_k)]_d^2)) \\
 &= -\frac{\alpha}{2F_{\max}} \|\nabla f(W_k)\|_{H(W_k)}^2 \leq 0.
 \end{aligned} \tag{62}$$

Plugging (59) to (62) into (58), we bound the term (a) by

$$\begin{aligned}
 & \mathbb{E}_{\xi_k} [\langle \nabla f(W_k), W_{k+1} - W_k \rangle] \\
 &= -\frac{\alpha}{2F_{\max}} \|\nabla f(W_k)\|_{H(W_k)}^2 + \frac{\alpha\sigma^2}{2} \left\| \frac{G(W_k)}{\sqrt{F(W_k)}} \right\|_{\infty}^2 \\
 &\quad - \frac{1}{2\alpha F_{\max}} \mathbb{E}_{\xi_k} \left[\|W_{k+1} - W_k + \alpha(\nabla f(W_k; \xi_k) - \nabla f(W_k)) \odot F(W_k)\|^2 \right].
 \end{aligned} \tag{63}$$

Bound of the third term (b). The third term (b) in the RHS of (57) is bounded by

$$\frac{L}{2} \mathbb{E}_{\xi_k} [\|W_{k+1} - W_k\|^2] \tag{64}$$

$$\begin{aligned}
 &\leq L\mathbb{E}_{\xi_k} [\|W_{k+1} - W_k + \alpha(\nabla f(W_k; \xi_k) - \nabla f(W_k)) \odot F(W_k)\|^2] \\
 &\quad + \alpha^2 L\mathbb{E}_{\xi_k} [\|(\nabla f(W_k; \xi_k) - \nabla f(W_k)) \odot F(W_k)\|^2] \\
 &\leq L\mathbb{E}_{\xi_k} [\|W_{k+1} - W_k + \alpha(\nabla f(W_k; \xi_k) - \nabla f(W_k)) \odot F(W_k)\|^2] + \alpha^2 LF_{\max}^2 \sigma^2
 \end{aligned}$$

where the last inequality leverages the bounded variance of noise (Assumption 3.3) and the fact that $F(W_k)$ is bounded by F_{\max} element-wise.

Substituting (63) and (64) back into (57), we have

$$\begin{aligned}
 \mathbb{E}_{\xi_k} [f(W_{k+1})] &\leq f(W_k) - \frac{\alpha}{2F_{\max}} \|\nabla f(W_k)\|_{H(W_k)}^2 + \alpha^2 LF_{\max}^2 \sigma^2 + \frac{\alpha\sigma^2}{2} \left\| \frac{G(W_k)}{\sqrt{F(W_k)}} \right\|_{\infty}^2 \\
 &\quad - \frac{1}{F_{\max}} \left(\frac{1}{2\alpha} - LF_{\max} \right) \mathbb{E}_{\xi_k} [\|W_{k+1} - W_k + \alpha(\nabla f(W_k; \xi_k) - \nabla f(W_k)) \odot F(W_k)\|^2].
 \end{aligned} \tag{65}$$

The third term in the RHS of (65) can be bounded by

$$\begin{aligned}
 &\mathbb{E}_{\xi_k} [\|W_{k+1} - W_k + \alpha(\nabla f(W_k; \xi_k) - \nabla f(W_k)) \odot F(W_k)\|^2] \\
 &= \alpha^2 \mathbb{E}_{\xi_k} [\|\nabla f(W_k) \odot F(W_k) + |\nabla f(W_k; \xi_k)| \odot G(W_k)\|^2] \\
 &\geq \frac{1}{2} \alpha^2 \mathbb{E}_{\xi_k} [\|\nabla f(W_k) \odot F(W_k) + |\nabla f(W_k)| \odot G(W_k)\|^2] \\
 &\quad - \alpha^2 \mathbb{E}_{\xi_k} [\|(|\nabla f(W_k)| - |\nabla f(W_k; \xi_k)|) \odot G(W_k)\|^2] \\
 &\geq \frac{1}{2} \alpha^2 \mathbb{E}_{\xi_k} [\|\nabla f(W_k) \odot F(W_k) + |\nabla f(W_k)| \odot G(W_k)\|^2] \\
 &\quad - \alpha^2 \mathbb{E}_{\xi_k} [\|(\nabla f(W_k) - \nabla f(W_k; \xi_k)) \odot G(W_k)\|^2] \\
 &\geq \frac{1}{2} \alpha^2 \mathbb{E}_{\xi_k} [\|\nabla f(W_k) \odot F(W_k) + |\nabla f(W_k)| \odot G(W_k)\|^2] - \alpha^2 F_{\max} \sigma^2 \left\| \frac{G(W_k)}{\sqrt{F(W_k)}} \right\|_{\infty}^2
 \end{aligned} \tag{66}$$

where the first inequality holds because $\|x\|^2 \geq \frac{1}{2}\|x-y\|^2 - \|y\|^2$ for any $x, y \in \mathbb{R}^D$, the second inequality comes from $\|x\| - \|y\| \leq |x-y|$ for any $x, y \in \mathbb{R}$, and the last inequality holds because

$$\begin{aligned}
 &\mathbb{E}_{\xi_k} [\|(\nabla f(W_k) - \nabla f(W_k; \xi_k)) \odot G(W_k)\|^2] \\
 &= \mathbb{E}_{\xi_k} \left[\left\| (\nabla f(W_k) - \nabla f(W_k; \xi_k)) \odot \frac{G(W_k)}{\sqrt{F(W_k)}} \odot \sqrt{F(W_k)} \right\|^2 \right] \\
 &\leq F_{\max} \mathbb{E}_{\xi_k} \left[\left\| (\nabla f(W_k) - \nabla f(W_k; \xi_k)) \odot \frac{G(W_k)}{\sqrt{F(W_k)}} \right\|^2 \right] \\
 &\leq F_{\max} \mathbb{E}_{\xi_k} [\|\nabla f(W_k) - \nabla f(W_k; \xi_k)\|^2] \left\| \frac{G(W_k)}{\sqrt{F(W_k)}} \right\|_{\infty}^2 \\
 &\leq F_{\max} \sigma^2 \left\| \frac{G(W_k)}{\sqrt{F(W_k)}} \right\|_{\infty}^2.
 \end{aligned} \tag{67}$$

The learning rate $\alpha \leq \frac{1}{4LF_{\max}}$ implies that $\frac{1}{2\alpha} - LF_{\max} \leq \frac{1}{4\alpha}$ in (65), which leads (57) to

$$\begin{aligned}
 \mathbb{E}_{\xi_k} [f(W_{k+1})] &\leq f(W_k) - \frac{\alpha}{2F_{\max}} \|\nabla f(W_k)\|_{H(W_k)}^2 + \alpha^2 LF_{\max}^2 \sigma^2 + \alpha\sigma^2 \left\| \frac{G(W_k)}{\sqrt{F(W_k)}} \right\|_{\infty}^2 \\
 &\quad - \frac{\alpha}{8F_{\max}} \|\nabla f(W_k) \odot F(W_k) + |\nabla f(W_k)| \odot G(W_k)\|^2.
 \end{aligned} \tag{68}$$

Reorganizing (68), taking expectation over all $\xi_K, \xi_{K-1}, \dots, \xi_0$, and averaging them for k from 0 to $K - 1$ deduce that

$$\begin{aligned}
 E_K &= \frac{1}{K} \sum_{k=0}^{K-1} \mathbb{E}[\|\nabla f(W_k) \odot F(W_k) + |\nabla f(W_k)| \odot G(W_k)\|^2 + 4\|\nabla f(W_k)\|_{H(W_k)}^2] \\
 &\leq \frac{8F_{\max}(f(W_0) - \mathbb{E}[f(W_{K+1})])}{\alpha K} + 8\alpha L F_{\max}^3 \sigma^2 + 8F_{\max} \sigma^2 \times \frac{1}{K} \sum_{k=0}^{K-1} \left\| \frac{G(W_k)}{\sqrt{F(W_k)}} \right\|_{\infty}^2 \\
 &\leq \frac{8F_{\max}(f(W_0) - f^*)}{\alpha K} + 8\alpha L F_{\max}^3 \sigma^2 + 8F_{\max} \sigma^2 \times \frac{1}{K} \sum_{k=0}^{K-1} \left\| \frac{G(W_k)}{\sqrt{F(W_k)}} \right\|_{\infty}^2 \\
 &= 16F_{\max}^2 \sqrt{\frac{(f(W_0) - f^*)\sigma^2 L}{K}} + 8F_{\max} \sigma^2 S_K^{\text{ASGD}}
 \end{aligned} \tag{69}$$

where the last equality chooses the learning rate as $\alpha = \frac{1}{F_{\max}} \sqrt{\frac{f(W_0) - f^*}{\sigma^2 L K}}$. The proof is completed. \square

Remark F.1 (Tighter bound without saturation). Assuming the saturation never happens during the training, i.e. $H(W_k) \geq H_{\min}^{\text{TT}} > 0$ for all $k \in [K]$, we get a tighter bound in (68) by leveraging $\|\nabla f(W_k)\|_{H(W_k)}^2 \geq \min\{H(W_k)\} \|\nabla f(W_k)\|^2 \geq H_{\min}^{\text{TT}} \|\nabla f(W_k)\|^2$

$$\mathbb{E}_{\xi_k}[f(W_{k+1})] \leq f(W_k) - \frac{\alpha}{2F_{\max}} \|\nabla f(W_k)\|_{H(W_k)}^2 + \alpha^2 L F_{\max}^2 \sigma^2 + \alpha \sigma^2 \left\| \frac{G(W_k)}{\sqrt{F(W_k)}} \right\|_{\infty}^2 \tag{70}$$

which leads to

$$\begin{aligned}
 &\frac{1}{K} \sum_{k=0}^{K-1} [\|\nabla f(W_k)\|^2] \\
 &= \frac{4F_{\max}^2}{H_{\min}^{\text{TT}}} \sqrt{\frac{(f(W_0) - f^*)\sigma^2 L}{K}} + 2F_{\max} \sigma^2 \times \frac{1}{K} \sum_{k=0}^{K-1} \left\| \frac{G(W_k)}{\sqrt{F(W_k)}} \right\|_{\infty}^2 / \min\{H(W_k)\}.
 \end{aligned} \tag{71}$$

It exactly reduces to the result for the convergence of Analog SGD in (Wu et al., 2024a) on special linear response functions, as discussed in Appendix B.

G. Proof of Theorem 4.2: Convergence of Tiki-Taka

This section provides the convergence guarantee of the Tiki-Taka under the strongly convex assumption.

Theorem 4.2 (Convergence of Tiki-Taka). *Under Assumptions 3.2–3.4, and 4.1, with learning rate $\alpha = O(\sqrt{1/\sigma^2 K})$, $\beta = O(\alpha\gamma^{3/2})$, it holds for Tiki-Taka that*

$$E_K^{\text{TT}} \leq O\left(\sqrt{\sigma^2/K} + \sigma^2 S_K^{\text{TT}}\right) \tag{20}$$

where S_K^{TT} denotes the amplification factor of P_k given by $S_K^{\text{TT}} := \frac{1}{K} \sum_{k=0}^{K-1} \left\| \frac{G(P_k)}{\sqrt{F(P_k)}} \right\|_{\infty}^2$.

G.1. Main proof

Proof of Theorem 4.2. The proof of the Tiki-Taka convergence relies on the following two lemmas, which provide the sufficient descent of W_k and \bar{W}_k , respectively.

Lemma G.1 (Descent Lemma of \bar{W}_k). *Suppose Assumptions 3.2–3.3 hold. It holds for Tiki-Taka that*

$$\mathbb{E}_{\xi_k}[f(\bar{W}_{k+1})] \leq f(\bar{W}_k) - \frac{\alpha}{4F_{\max}} \|\nabla f(\bar{W}_k)\|_{H(P_k)}^2 + 2\alpha \sigma^2 \left\| \frac{G(P_k)}{\sqrt{F(P_k)}} \right\|_{\infty}^2 + 2\alpha^2 L F_{\max}^2 \sigma^2 \tag{72}$$

$$\begin{aligned}
 & - \frac{\alpha\gamma}{8F_{\max}} \|\nabla f(\bar{W}_k) \odot F(P_k) + |\nabla f(\bar{W}_k)| \odot G(P_k)\|^2 \\
 & + \frac{F_{\max}}{\alpha} \mathbb{E}_{\xi_k} \left[\|W_{k+1} - W_k\|_{H(P_k)^\dagger}^2 \right] + \mathbb{E}_{\xi_k} [\|W_{k+1} - W_k\|^2].
 \end{aligned}$$

Lemma G.2 (Descent Lemma of W_k). *It holds for Tiki-Taka that*

$$\begin{aligned}
 \|W_{k+1} - W^*\|^2 & \leq \|W_k - W^*\|^2 - \frac{\beta}{2\gamma F_{\max}} \|W_k - W^*\|_{H(W_k)}^2 \\
 & - \frac{\beta\gamma}{2F_{\max}} \|P^*(W_k) \odot F(W_k) - |P^*(W_k)| \odot G(W_k)\|^2 \\
 & + \frac{2\beta F_{\max}^3}{\gamma} \|P_{k+1} - P^*(W_k)\|_{H(W_k)^\dagger}^2 + 2\beta^2 \|P_{k+1} - P^*(W_k)\|^2.
 \end{aligned} \tag{73}$$

The proof of Lemma G.1 and G.2 are deferred to Section G.2 and G.3, respectively.

For a sufficiently large γ , $P^*(W_k)$ is ensured to be located in the dynamic range of analog tile P_k and hence the constraint in (15) is never active. Therefore, we may assume both $q_+(P_k)$ and $q_-(P_k)$ are non-zero, equivalently, there exists a non-zero constant H_{\min}^{TT} such that $\min\{H(P_k)\} \geq H_{\min}^{\text{TT}}$ for all k . Under this condition, we have the following inequalities

$$\frac{\alpha}{4F_{\max}} \|\nabla f(\bar{W}_k)\|_{H(P_k)}^2 \geq \frac{\alpha H_{\min}^{\text{TT}}}{4F_{\max}} \|\nabla f(\bar{W}_k)\|^2, \tag{74}$$

$$\frac{F_{\max}}{\alpha\gamma} \|W_{k+1} - W_k\|_{H(P_k)^\dagger}^2 \leq \frac{F_{\max}}{\alpha\gamma H_{\min}^{\text{TT}}} \|W_{k+1} - W_k\|^2. \tag{75}$$

Similarly, we bound the term $\|P_{k+1} - P^*(W_k)\|_{H(W_k)^\dagger}^2$ in (72) by

$$\frac{2\beta F_{\max}^3}{\gamma} \|P_{k+1} - P^*(W_k)\|_{H(W_k)^\dagger}^2 \leq \frac{2\beta F_{\max}^3}{\gamma \min\{H(W_k)\}} \|P_{k+1} - P^*(W_k)\|^2. \tag{76}$$

Notice it is only required to have $\min\{H(W_k)\} > 0$ for the inequality to hold.

By inequality (75), the last two terms in the RHS of (72) is bounded by

$$\begin{aligned}
 & \frac{F_{\max}}{\alpha} \mathbb{E}_{\xi_k} \left[\|W_{k+1} - W_k\|_{H(P_k)^\dagger}^2 \right] + \mathbb{E}_{\xi_k} [\|W_{k+1} - W_k\|^2] \\
 & = \frac{F_{\max}}{\alpha H_{\min}^{\text{TT}}} \mathbb{E}_{\xi_k} [\|W_{k+1} - W_k\|^2] + \mathbb{E}_{\xi_k} [\|W_{k+1} - W_k\|^2] \\
 & \stackrel{(a)}{\leq} \frac{2F_{\max}}{\alpha H_{\min}^{\text{TT}}} \mathbb{E}_{\xi_k} [\|W_{k+1} - W_k\|^2] = \frac{2\beta^2 F_{\max}}{\alpha H_{\min}^{\text{TT}}} \|P_{k+1} \odot F(W_k) - |P_{k+1}| \odot G(W_k)\|^2 \\
 & \leq \frac{4\beta^2 F_{\max}}{\alpha H_{\min}^{\text{TT}}} \|P^*(W_k) \odot F(W_k) - |P^*(W_k)| \odot G(W_k)\|^2 \\
 & \quad + \frac{4\beta^2 F_{\max}}{\alpha H_{\min}^{\text{TT}}} \|P_{k+1} \odot F(W_k) - |P_{k+1}| \odot G(W_k) - (P^*(W_k) \odot F(W_k) - |P^*(W_k)| \odot G(W_k))\|^2 \\
 & \stackrel{(b)}{\leq} \frac{4\beta^2 F_{\max}}{\alpha H_{\min}^{\text{TT}}} \|P^*(W_k) \odot F(W_k) - |P^*(W_k)| \odot G(W_k)\|^2 + \frac{4\beta^2 F_{\max}}{\alpha H_{\min}^{\text{TT}}} \|P_{k+1} - P^*(W_k)\|^2.
 \end{aligned} \tag{77}$$

where (a) holds if learning rate α is sufficiently small such that $\frac{F_{\max}}{\alpha\gamma H_{\min}^{\text{TT}}} \geq 1$; (b) comes from the Lipschitz continuity of the analog update (c.f. Lemma C.3).

With all the inequalities and lemmas above, we are ready to prove the main conclusion in Theorem 4.2 now. Define a Lyapunov function by

$$\mathbb{V}_k := f(\bar{W}_k) - f^* + C\|W_k - W^*\|^2. \tag{78}$$

By Lemmas G.1 and G.2, we show that \mathbb{V}_k has sufficient descent in expectation

$$\begin{aligned}
 & \mathbb{E}_{\xi_k} [\mathbb{V}_{k+1}] \\
 &= \mathbb{E}_{\xi_k} [f(\bar{W}_{k+1}) - f^* + C\|W_{k+1} - W^*\|^2] \\
 &\leq f(\bar{W}_k) - f^* - \frac{\alpha}{4F_{\max}} \|\nabla f(\bar{W}_k)\|_{H(P_k)}^2 + 2\alpha\sigma^2 \left\| \frac{G(P_k)}{\sqrt{F(P_k)}} \right\|_{\infty}^2 + 2\alpha^2 L F_{\max}^2 \sigma^2 \\
 &\quad - \frac{\alpha}{8F_{\max}} \|\nabla f(\bar{W}_k) \odot F(P_k) + |\nabla f(\bar{W}_k)| \odot G(P_k)\|^2 \\
 &\quad + \frac{4\beta^2 F_{\max}}{\alpha H_{\min}^{\text{TT}}} \|P^*(W_k) \odot F(W_k) - |P^*(W_k)| \odot G(W_k)\|^2 + \frac{4\beta^2 F_{\max}}{\alpha H_{\min}^{\text{TT}}} \mathbb{E}_{\xi_k} [\|P_{k+1} - P^*(W_k)\|^2] \\
 &\quad + C \left(\|W_k - W^*\|^2 - \frac{\beta}{2\gamma F_{\max}} \|W_k - W^*\|_{H(W_k)}^2 + \frac{3\beta F_{\max}^3}{\gamma \min\{H(W_k)\}} \mathbb{E}_{\xi_k} [\|P_{k+1} - P^*(W_k)\|^2] \right. \\
 &\quad \left. - \frac{\beta\gamma}{2F_{\max}} \|P^*(W_k) \odot F(W_k) - |P^*(W_k)| \odot G(W_k)\|^2 \right) \\
 &\leq \mathbb{V}_k - \frac{\alpha H_{\min}^{\text{TT}}}{4F_{\max}} \|\nabla f(\bar{W}_k)\|^2 + 2\alpha\sigma^2 \left\| \frac{G(P_k)}{\sqrt{F(P_k)}} \right\|_{\infty}^2 + 2\alpha^2 L F_{\max}^2 \sigma^2 \\
 &\quad - \frac{\alpha}{8F_{\max}} \|\nabla f(\bar{W}_k) \odot F(P_k) + |\nabla f(\bar{W}_k)| \odot G(P_k)\|^2 \\
 &\quad - \left(\frac{\beta\gamma}{2F_{\max}} C - \frac{4\beta^2 F_{\max}}{\alpha H_{\min}^{\text{TT}}} \right) \|P^*(W_k) \odot F(W_k) - |P^*(W_k)| \odot G(W_k)\|^2 \\
 &\quad + \left(\frac{3\beta F_{\max}^3}{\gamma \min\{H(W_k)\}} C + \frac{4\beta^2 F_{\max}}{\alpha H_{\min}^{\text{TT}}} \right) \mathbb{E}_{\xi_k} [\|P_{k+1} - P^*(W_k)\|^2] - \frac{\beta}{2\gamma F_{\max}} C \|W_k - W^*\|_{H(W_k)}^2.
 \end{aligned} \tag{79}$$

Let $C = \frac{10\beta F_{\max}^2}{\alpha H_{\min}^{\text{TT}} \gamma}$, which leads to the positive coefficient in front of $\|P_{k+1} - P^*(W_k)\|^2$, i.e.

$$\begin{aligned}
 & \mathbb{E}_{\xi_k} [\mathbb{V}_{k+1}] \\
 &\leq \mathbb{V}_k - \frac{\alpha H_{\min}^{\text{TT}}}{4F_{\max}} \|\nabla f(\bar{W}_k)\|^2 + 2\alpha\sigma^2 \left\| \frac{G(P_k)}{\sqrt{F(P_k)}} \right\|_{\infty}^2 + 2\alpha^2 L F_{\max}^2 \sigma^2 \\
 &\quad - \frac{\alpha}{8F_{\max}} \|\nabla f(\bar{W}_k) \odot F(P_k) + |\nabla f(\bar{W}_k)| \odot G(P_k)\|^2 \\
 &\quad - \frac{\beta^2 F_{\max}}{\alpha H_{\min}^{\text{TT}}} \|P^*(W_k) \odot F(W_k) - |P^*(W_k)| \odot G(W_k)\|^2 \\
 &\quad + \left(\frac{30\beta^2 F_{\max}^5}{\alpha\gamma \min\{H(W_k)\} H_{\min}^{\text{TT}}} + \frac{4\beta^2 F_{\max}}{\alpha H_{\min}^{\text{TT}}} \right) \mathbb{E}_{\xi_k} [\|P_{k+1} - P^*(W_k)\|^2] - \frac{5\beta^2 F_{\max}}{\alpha H_{\min}^{\text{TT}}} \|W_k - W^*\|_{H(W_k)}^2.
 \end{aligned} \tag{80}$$

Notice that the $\|P_{k+1} - P^*(W_k)\|^2$ appears in the RHS above, we also need the following lemma to bound it in terms of $\|P_k - P^*(W_k)\|^2$.

Lemma G.3 (Descent Lemma of P_k). *Suppose Assumptions 2.2-3.3 and 4.1 hold. It holds for Tiki-Taka that*

$$\begin{aligned}
 & \mathbb{E}_{\xi_k} [\|P_{k+1} - P^*(W_k)\|^2] \\
 &\leq \left(1 - \frac{\alpha\gamma\mu L}{4(\mu + L)} \right) \|P_k - P^*(W_k)\|^2 + \frac{2\alpha(\mu + L)F_{\max}\sigma^2}{\gamma\mu L} \left\| \frac{G(P_k)}{\sqrt{F(P_k)}} \right\|_{\infty}^2 + \alpha^2 F_{\max}^2 \sigma^2.
 \end{aligned} \tag{81}$$

The proof of Lemma G.3 is deferred to Section G.4. By Lemma G.3, we bound the $\|P_{k+1} - P^*(W_k)\|^2$ in terms of $\|P_k - P^*(W_k)\|^2$ as

$$\left(\frac{30\beta^2 F_{\max}^5}{\alpha\gamma \min\{H(W_k)\} H_{\min}^{\text{TT}}} + \frac{4\beta^2 F_{\max}}{\alpha H_{\min}^{\text{TT}}} \right) \mathbb{E}_{\xi_k} [\|P_{k+1} - P^*(W_k)\|^2] \tag{82}$$

$$\begin{aligned}
 &\stackrel{(a)}{\leq} \frac{32\beta^2 F_{\max}^5}{\alpha\gamma \min\{H(W_k)\} H_{\min}^{\text{TT}}} \mathbb{E}_{\xi_k} [\|P_{k+1} - P^*(W_k)\|^2] \\
 &\leq \frac{32\beta^2 F_{\max}^5}{\alpha\gamma \min\{H(W_k)\} H_{\min}^{\text{TT}}} \left(1 - \frac{\alpha}{4} \frac{\mu L}{\gamma(\mu + L)}\right) \|P_k - P^*(W_k)\|^2 \\
 &\quad + \frac{32\beta^2 F_{\max}^5}{\alpha\gamma \min\{H(W_k)\} H_{\min}^{\text{TT}}} \left(\frac{2\alpha(\mu + L)F_{\max}\sigma^2}{\gamma\mu L} \left\|\frac{G(P_k)}{\sqrt{F(P_k)}}\right\|_{\infty}^2 + \alpha^2 F_{\max}^2 \sigma^2\right) \\
 &\leq \frac{32\beta^2 F_{\max}^5}{\alpha\gamma \min\{H(W_k)\} H_{\min}^{\text{TT}}} \|P_k - P^*(W_k)\|^2 + O\left(\beta^2 \sigma^2 \left\|\frac{G(P_k)}{\sqrt{F(P_k)}}\right\|_{\infty}^2 + \alpha\beta^2 F_{\max}^2 \sigma^2\right) \\
 &\stackrel{(b)}{\leq} \frac{32\beta^2 F_{\max}^5}{\alpha\gamma \min\{H(W_k)\} H_{\min}^{\text{TT}}} \|P_k - P^*(W_k)\|^2 + \alpha\sigma^2 \left\|\frac{G(P_k)}{\sqrt{F(P_k)}}\right\|_{\infty}^2 + \alpha^2 L F_{\max}^2 \sigma^2
 \end{aligned}$$

where (a) assumes $\frac{4\beta^2 F_{\max}}{\alpha H_{\min}^{\text{TT}}} \leq \frac{2\beta^2 F_{\max}^5}{\alpha\gamma \min\{H(W_k)\} H_{\min}^{\text{TT}}}$ with lost of generality to keep the formulations simple since $\gamma \min\{H(W_k)\}$ is typically small; (b) holds given α and β is sufficiently small. In addition, the strong convexity of the objective (c.f. Assumption 4.1) implies that

$$\begin{aligned}
 \frac{\alpha H_{\min}^{\text{TT}}}{8F_{\max}} \|\nabla f(\bar{W}_k)\|^2 &\geq \frac{\alpha\mu^2 H_{\min}^{\text{TT}}}{8F_{\max}} \|\bar{W}_k - W^*\|^2 = \frac{\alpha\mu^2 H_{\min}^{\text{TT}}}{8F_{\max}} \|W_k + \gamma P_k - W^*\|^2 \\
 &= \frac{\alpha\mu^2 \gamma^2 H_{\min}^{\text{TT}}}{8F_{\max}} \left\|P_k - \frac{W^* - W_k}{\gamma}\right\|^2 = \frac{\alpha\mu^2 \gamma^2 H_{\min}^{\text{TT}}}{8F_{\max}} \|P_k - P^*(W_k)\|^2.
 \end{aligned} \tag{83}$$

Substituting (82) and (83) back into (80) yields

$$\begin{aligned}
 &\mathbb{E}_{\xi_k} [\mathbb{V}_{k+1}] \\
 &\leq \mathbb{V}_k - \frac{\alpha H_{\min}^{\text{TT}}}{8F_{\max}} \|\nabla f(\bar{W}_k)\|^2 + 3\alpha\sigma^2 \left\|\frac{G(P_k)}{\sqrt{F(P_k)}}\right\|_{\infty}^2 + 3\alpha^2 L F_{\max}^2 \sigma^2 \\
 &\quad - \frac{\alpha}{8F_{\max}} \|\nabla f(\bar{W}_k) \odot F(P_k) + |\nabla f(\bar{W}_k)| \odot G(P_k)\|^2 \\
 &\quad - \frac{\beta^2 F_{\max}}{\alpha H_{\min}^{\text{TT}}} \|P^*(W_k) \odot F(W_k) - |P^*(W_k)| \odot G(W_k)\|^2 \\
 &\quad - \left(\frac{\alpha\mu^2 \gamma^2}{8F_{\max} H_{\min}^{\text{TT}}} - \frac{32\beta^2 F_{\max}^5}{\alpha\gamma \min\{H(W_k)\} H_{\min}^{\text{TT}}}\right) \|P_k - P^*(W_k)\|^2 - \frac{5\beta^2 F_{\max}}{\alpha H_{\min}^{\text{TT}}} \|W_k - W^*\|_{H(W_k)}^2 \\
 &= \mathbb{V}_k - \frac{\alpha H_{\min}^{\text{TT}}}{8F_{\max}} \|\nabla f(\bar{W}_k)\|^2 + 3\alpha\sigma^2 \left\|\frac{G(P_k)}{\sqrt{F(P_k)}}\right\|_{\infty}^2 + 3\alpha^2 L F_{\max}^2 \sigma^2 \\
 &\quad - \frac{\alpha}{8F_{\max}} \|\nabla f(\bar{W}_k) \odot F(P_k) + |\nabla f(\bar{W}_k)| \odot G(P_k)\|^2 \\
 &\quad - \frac{\alpha\mu^2 \gamma^3 \min\{H(W_k)\}}{512F_{\max}^5 H_{\min}^{\text{TT}}} \|P^*(W_k) \odot F(W_k) - |P^*(W_k)| \odot G(W_k)\|^2 \\
 &\quad - \frac{\alpha\mu^2 \gamma^2}{16F_{\max} H_{\min}^{\text{TT}}} \|P_k - P^*(W_k)\|^2 - \frac{5\alpha\mu^2 \gamma^3}{512F_{\max}^5 H_{\min}^{\text{TT}}} \|W_k - W^*\|_{H(W_k)}^2
 \end{aligned} \tag{84}$$

where the last step chooses the learning rate by

$$\beta = \frac{\alpha\mu\gamma^{\frac{3}{2}} \sqrt{\min\{H(W_k)\}}}{16\sqrt{2}F_{\max}^3}. \tag{85}$$

Rearranging inequality (79) above, we have

$$\frac{\alpha}{8F_{\max}} \|\nabla f(\bar{W}_k) \odot F(P_k) + |\nabla f(\bar{W}_k)| \odot G(P_k)\|^2 + \frac{\alpha}{8F_{\max} H_{\min}^{\text{TT}}} \|\nabla f(\bar{W}_k)\|^2 \tag{86}$$

$$\begin{aligned}
 & + \frac{\alpha\mu^2\gamma^3 \min\{H(W_k)\}}{512F_{\max}^5 H_{\min}^{\text{TT}}} \|P^*(W_k) \odot F(W_k) - |P^*(W_k)| \odot G(W_k)\|^2 \\
 & + \frac{5\alpha\mu^2\gamma^3 \min\{H(W_k)\}}{512F_{\max}^5 H_{\min}^{\text{TT}}} \|W_k - W^*\|_{H(W_k)}^2 + \frac{\alpha\mu^2\gamma^2}{16F_{\max} H_{\min}^{\text{TT}}} \|P_k - P^*(W_k)\|^2 \\
 & \leq \mathbb{V}_k - \mathbb{E}_{\xi_k}[\mathbb{V}_{k+1}] + 3\alpha^2 L F_{\max}^2 \sigma^2 + 3\alpha\sigma^2 \left\| \frac{G(P_k)}{\sqrt{F(P_k)}} \right\|_{\infty}^2.
 \end{aligned}$$

Define the convergence metric E_K^{TT} as

$$\begin{aligned}
 E_K^{\text{TT}} := & \frac{1}{K} \sum_{k=0}^{K-1} \mathbb{E} \left[\|\nabla f(\bar{W}_k) \odot F(P_k) + |\nabla f(\bar{W}_k)| \odot G(P_k)\|^2 + \frac{1}{H_{\min}^{\text{TT}}} \|\nabla f(\bar{W}_k)\|^2 \right. \\
 & + \frac{\mu^2\gamma^3 \min\{H(W_k)\}}{64F_{\max}^4 H_{\min}^{\text{TT}}} \|P^*(W_k) \odot F(W_k) - |P^*(W_k)| \odot G(W_k)\|^2 \\
 & \left. + \frac{5\mu^2\gamma^3}{64F_{\max}^4 H_{\min}^{\text{TT}}} \|W_k - W^*\|_{H(W_k)}^2 + \frac{\mu^2\gamma^2}{2H_{\min}^{\text{TT}}} \|P_k - P^*(W_k)\|^2 \right]. \tag{87}
 \end{aligned}$$

Taking expectation over all $\xi_K, \xi_{K-1}, \dots, \xi_0$, averaging (86) over k from 0 to $K-1$, and choosing the parameter α as $\alpha = O\left(\frac{1}{F_{\max}} \sqrt{\frac{\mathbb{V}_0}{\sigma^2 L K}}\right)$ deduce that

$$\begin{aligned}
 E_K^{\text{TT}} & \leq 8F_{\max} \left(\frac{\mathbb{V}_0 - \mathbb{E}[\mathbb{V}_{k+1}]}{\alpha K} + 3\alpha L F_{\max}^2 \sigma^2 \right) + 24F_{\max} \sigma^2 \times \frac{1}{K} \sum_{k=0}^{K-1} \left\| \frac{G(P_k)}{\sqrt{F(P_k)}} \right\|_{\infty}^2 \\
 & \leq 8F_{\max} \left(\frac{\mathbb{V}_0}{\alpha K} + 3\alpha L F_{\max}^2 \sigma^2 \right) + 24F_{\max} \sigma^2 \times \frac{1}{K} \sum_{k=0}^{K-1} \left\| \frac{G(P_k)}{\sqrt{F(P_k)}} \right\|_{\infty}^2 \\
 & = O\left(F_{\max}^2 \sqrt{\frac{\mathbb{V}_0 \sigma^2 L}{K}}\right) + 24F_{\max} \sigma^2 S_K^{\text{TT}}. \tag{88}
 \end{aligned}$$

The strong convexity of the objective (Assumption 4.1) implies that

$$\mathbb{V}_0 = f(\bar{W}_0) - f^* + C\|W_0 - W^*\|^2 \leq \left(1 + \frac{2C}{\mu}\right) (f(W_0) - f^*). \tag{89}$$

Plugging it back to the above inequality, we have

$$E_K^{\text{TT}} = O\left(F_{\max}^2 \sqrt{\frac{(f(W_0) - f^*)\sigma^2 L}{K}}\right) + 24F_{\max} \sigma^2 S_K^{\text{TT}}. \tag{90}$$

The proof is completed. \square

G.2. Proof of Lemma G.1: Descent of sequence \bar{W}_k

Lemma G.1 (Descent Lemma of \bar{W}_k). *Suppose Assumptions 3.2–3.3 hold. It holds for Tiki-Taka that*

$$\begin{aligned}
 \mathbb{E}_{\xi_k}[f(\bar{W}_{k+1})] & \leq f(\bar{W}_k) - \frac{\alpha}{4F_{\max}} \|\nabla f(\bar{W}_k)\|_{H(P_k)}^2 + 2\alpha\sigma^2 \left\| \frac{G(P_k)}{\sqrt{F(P_k)}} \right\|_{\infty}^2 + 2\alpha^2 L F_{\max}^2 \sigma^2 \\
 & \quad - \frac{\alpha\gamma}{8F_{\max}} \|\nabla f(\bar{W}_k) \odot F(P_k) + |\nabla f(\bar{W}_k)| \odot G(P_k)\|^2 \\
 & \quad + \frac{F_{\max}}{\alpha} \mathbb{E}_{\xi_k} \left[\|W_{k+1} - W_k\|_{H(P_k)^\dagger}^2 \right] + \mathbb{E}_{\xi_k} [\|W_{k+1} - W_k\|^2]. \tag{72}
 \end{aligned}$$

Proof of Lemma G.1. The L -smooth assumption (Assumption 3.2) implies that

$$\begin{aligned} \mathbb{E}_{\xi_k} [f(\bar{W}_{k+1})] &\leq f(\bar{W}_k) + \mathbb{E}_{\xi_k} [\langle \nabla f(\bar{W}_k), \bar{W}_{k+1} - \bar{W}_k \rangle] + \frac{L}{2} \mathbb{E}_{\xi_k} [\|\bar{W}_{k+1} - \bar{W}_k\|^2] \\ &= f(\bar{W}_k) + \underbrace{\gamma \mathbb{E}_{\xi_k} [\langle \nabla f(\bar{W}_k), P_{k+1} - P_k \rangle]}_{(a)} + \underbrace{\mathbb{E}_{\xi_k} [\langle \nabla f(\bar{W}_k), W_{k+1} - W_k \rangle]}_{(b)} + \underbrace{\frac{L}{2} \mathbb{E}_{\xi_k} [\|\bar{W}_{k+1} - \bar{W}_k\|^2]}_{(c)}. \end{aligned} \quad (91)$$

Next, we will handle the each term in the RHS of (91) separately.

Bound of the second term (a). To bound term (a) in the RHS of (91), we leverage the assumption that noise has expectation 0 (Assumption 3.3)

$$\begin{aligned} &\mathbb{E}_{\xi_k} [\langle \nabla f(\bar{W}_k), P_{k+1} - P_k \rangle] \\ &= \alpha \mathbb{E}_{\xi_k} \left[\left\langle \nabla f(\bar{W}_k) \odot \sqrt{F(P_k)}, \frac{P_{k+1} - P_k}{\alpha \sqrt{F(P_k)}} + (\nabla f(\bar{W}_k; \xi_k) - \nabla f(\bar{W}_k)) \odot \sqrt{F(P_k)} \right\rangle \right] \\ &= -\frac{\alpha}{2} \|\nabla f(\bar{W}_k) \odot \sqrt{F(P_k)}\|^2 \\ &\quad - \frac{1}{2\alpha} \mathbb{E}_{\xi_k} \left[\left\| \frac{P_{k+1} - P_k}{\sqrt{F(P_k)}} + \alpha (\nabla f(\bar{W}_k; \xi_k) - \nabla f(\bar{W}_k)) \odot \sqrt{F(P_k)} \right\|^2 \right] \\ &\quad + \frac{1}{2\alpha} \mathbb{E}_{\xi_k} \left[\left\| \frac{P_{k+1} - P_k}{\sqrt{F(P_k)}} + \alpha \nabla f(\bar{W}_k; \xi_k) \odot \sqrt{F(P_k)} \right\|^2 \right]. \end{aligned} \quad (92)$$

The second term in the RHS of (92) can be bounded by

$$\begin{aligned} &\frac{1}{2\alpha} \mathbb{E}_{\xi_k} \left[\left\| \frac{P_{k+1} - P_k}{\sqrt{F(P_k)}} + \alpha (\nabla f(\bar{W}_k; \xi_k) - \nabla f(\bar{W}_k)) \odot \sqrt{F(P_k)} \right\|^2 \right] \\ &= \frac{1}{2\alpha} \mathbb{E}_{\xi_k} \left[\left\| \frac{P_{k+1} - P_k + \alpha (\nabla f(\bar{W}_k; \xi_k) - \nabla f(\bar{W}_k)) \odot F(P_k)}{\sqrt{F(P_k)}} \right\|^2 \right] \\ &\geq \frac{1}{2\alpha F_{\max}} \mathbb{E}_{\xi_k} [\|P_{k+1} - P_k + \alpha (\nabla f(\bar{W}_k; \xi_k) - \nabla f(\bar{W}_k)) \odot F(P_k)\|^2]. \end{aligned} \quad (93)$$

The third term in the RHS of (92) can be bounded by variance decomposition and bounded variance assumption (Assumption 3.3)

$$\begin{aligned} &\frac{1}{2\alpha} \mathbb{E}_{\xi_k} \left[\left\| \frac{P_{k+1} - P_k}{\sqrt{F(P_k)}} + \alpha \nabla f(\bar{W}_k; \xi_k) \odot \sqrt{F(P_k)} \right\|^2 \right] \\ &\leq \frac{\alpha}{2} \mathbb{E}_{\xi_k} \left[\left\| |\nabla f(\bar{W}_k; \xi_k)| \odot \frac{G(P_k)}{\sqrt{F(P_k)}} \right\|^2 \right] \\ &\leq \frac{\alpha}{2} \left\| |\nabla f(\bar{W}_k)| \odot \frac{G(P_k)}{\sqrt{F(P_k)}} \right\|^2 + \frac{\alpha \sigma^2}{2} \left\| \frac{G(P_k)}{\sqrt{F(P_k)}} \right\|_{\infty}^2. \end{aligned} \quad (94)$$

Notice that the first term in the RHS of (92) and the second term in the RHS of (94) can be bounded together

$$-\frac{\alpha}{2} \|\nabla f(\bar{W}_k) \odot \sqrt{F(P_k)}\|^2 + \frac{\alpha}{2} \left\| |\nabla f(\bar{W}_k)| \odot \frac{G(P_k)}{\sqrt{F(P_k)}} \right\|^2 \quad (95)$$

$$\begin{aligned}
 &= -\frac{\alpha}{2} \sum_{d \in [D]} \left([\nabla f(\bar{W}_k)]_d^2 \left([F(P_k)]_d - \frac{[G(P_k)]_d^2}{[F(P_k)]_d} \right) \right) \\
 &= -\frac{\alpha}{2} \sum_{d \in [D]} \left([\nabla f(\bar{W}_k)]_d^2 \left(\frac{[F(P_k)]_d^2 - [G(P_k)]_d^2}{[F(P_k)]_d} \right) \right) \\
 &\leq -\frac{\alpha}{2F_{\max}} \sum_{d \in [D]} ([\nabla f(\bar{W}_k)]_d^2 ([F(P_k)]_d^2 - [G(P_k)]_d^2)) \\
 &= -\frac{\alpha}{2F_{\max}} \|\nabla f(\bar{W}_k)\|_{H(P_k)}^2 \leq 0.
 \end{aligned}$$

Plugging (93) to (95) into (92), we bound the term (a) by

$$\begin{aligned}
 &\mathbb{E}_{\xi_k} [\langle \nabla f(\bar{W}_k), P_{k+1} - P_k \rangle] \\
 &\leq -\frac{\alpha}{2F_{\max}} \|\nabla f(\bar{W}_k)\|_{H(P_k)}^2 + \frac{\alpha\sigma^2}{2} \left\| \frac{G(P_k)}{\sqrt{F(P_k)}} \right\|_{\infty}^2 \\
 &\quad - \frac{1}{2\alpha F_{\max}} \mathbb{E}_{\xi_k} \left[\left\| P_{k+1} - P_k + \alpha(\nabla f(\bar{W}_k; \xi_k) - \nabla f(\bar{W}_k)) \odot F(P_k) \right\|^2 \right].
 \end{aligned} \tag{96}$$

Bound of the third term (b). By Young's inequality, we have

$$\mathbb{E}_{\xi_k} [\langle \nabla f(\bar{W}_k), W_{k+1} - W_k \rangle] \leq \frac{\alpha}{4F_{\max}} \|\nabla f(\bar{W}_k)\|_{H(P_k)}^2 + \frac{F_{\max}}{\alpha} \mathbb{E}_{\xi_k} [\|W_{k+1} - W_k\|_{H(P_k)}^2]. \tag{97}$$

Bound of the third term (c). Repeatedly applying inequality $\|U + V\|^2 \leq 2\|U\|^2 + 2\|V\|^2$ for any $U, V \in \mathbb{R}^D$, we have

$$\begin{aligned}
 &\frac{L}{2} \mathbb{E}_{\xi_k} [\|\bar{W}_{k+1} - \bar{W}_k\|^2] \\
 &\leq L \mathbb{E}_{\xi_k} [\|W_{k+1} - W_k\|^2] + L \mathbb{E}_{\xi_k} [\|P_{k+1} - P_k\|^2] \\
 &\leq L \mathbb{E}_{\xi_k} [\|W_{k+1} - W_k\|^2] + 2L \mathbb{E}_{\xi_k} \left[\left\| P_{k+1} - P_k + \alpha(\nabla f(\bar{W}_k; \xi_k) - \nabla f(\bar{W}_k)) \odot F(P_k) \right\|^2 \right] \\
 &\quad + 2\alpha^2 L \mathbb{E}_{\xi_k} \left[\left\| (\nabla f(\bar{W}_k; \xi_k) - \nabla f(\bar{W}_k)) \odot F(P_k) \right\|^2 \right] \\
 &\leq \mathbb{E}_{\xi_k} [\|W_{k+1} - W_k\|^2] + 2L \mathbb{E}_{\xi_k} \left[\left\| P_{k+1} - P_k + \alpha(\nabla f(\bar{W}_k; \xi_k) - \nabla f(\bar{W}_k)) \odot F(P_k) \right\|^2 \right] \\
 &\quad + 2\alpha^2 L F_{\max}^2 \sigma^2
 \end{aligned} \tag{98}$$

where the last inequality comes from the bounded variance assumption (Assumption 3.3)

$$\begin{aligned}
 &2\alpha^2 L \mathbb{E}_{\xi_k} \left[\left\| (\nabla f(\bar{W}_k; \xi_k) - \nabla f(\bar{W}_k)) \odot F(P_k) \right\|^2 \right] \\
 &\leq 2\alpha^2 L F_{\max}^2 \mathbb{E}_{\xi_k} \left[\left\| \nabla f(\bar{W}_k; \xi_k) - \nabla f(\bar{W}_k) \right\|^2 \right] \\
 &\leq 2\alpha^2 L F_{\max}^2 \sigma^2.
 \end{aligned} \tag{99}$$

Combination of the upper bound (a), (b), and (c). Plugging (96), (97), (98) into (91), we derive

$$\begin{aligned}
 \mathbb{E}_{\xi_k} [f(\bar{W}_{k+1})] &\leq f(\bar{W}_k) - \frac{\alpha}{4F_{\max}} \|\nabla f(\bar{W}_k)\|_{H(P_k)}^2 + \frac{\alpha\sigma^2}{2} \left\| \frac{G(P_k)}{\sqrt{F(P_k)}} \right\|_{\infty}^2 \\
 &\quad - \left(\frac{1}{2\alpha F_{\max}} - 2L \right) \mathbb{E}_{\xi_k} \left[\left\| P_{k+1} - P_k + \alpha(\nabla f(\bar{W}_k; \xi_k) - \nabla f(\bar{W}_k)) \odot F(P_k) \right\|^2 \right] \\
 &\quad + \frac{F_{\max}}{\alpha} \mathbb{E}_{\xi_k} \left[\|W_{k+1} - W_k\|_{H(P_k)}^2 \right] + \mathbb{E}_{\xi_k} [\|W_{k+1} - W_k\|^2] + 2\alpha^2 L F_{\max}^2 \sigma^2.
 \end{aligned} \tag{100}$$

We bound the fourth term in the RHS of (100) using the similar technique as in (66)

$$\begin{aligned} & \mathbb{E}_{\xi_k} \left[\left\| P_{k+1} - P_k + \alpha (\nabla f(\bar{W}_k; \xi_k) - \nabla f(\bar{W}_k)) \odot F(P_k) \right\|^2 \right] \\ & \geq \frac{\alpha^2}{2} \left\| \nabla f(\bar{W}_k) \odot F(P_k) + |\nabla f(\bar{W}_k)| \odot G(P_k) \right\|^2 - \alpha^2 F_{\max} \sigma^2 \left\| \frac{G(P_k)}{\sqrt{F(P_k)}} \right\|_{\infty}^2. \end{aligned} \quad (101)$$

Inequality (101) as well as the learning rate rule $\alpha \leq \frac{1}{4LF_{\max}}$ leads to the conclusion

$$\begin{aligned} \mathbb{E}_{\xi_k} [f(\bar{W}_{k+1})] & \leq f(\bar{W}_k) - \frac{\alpha}{4F_{\max}} \|\nabla f(\bar{W}_k)\|_{H(P_k)}^2 + 2\alpha\sigma^2 \left\| \frac{G(P_k)}{\sqrt{F(P_k)}} \right\|_{\infty}^2 + 2\alpha^2 LF_{\max}^2 \sigma^2 \\ & \quad - \frac{\alpha\gamma}{8F_{\max}} \|\nabla f(\bar{W}_k) \odot F(P_k) + |\nabla f(\bar{W}_k)| \odot G(P_k)\|^2 \\ & \quad + \frac{F_{\max}}{\alpha} \mathbb{E}_{\xi_k} \left[\|W_{k+1} - W_k\|_{H(P_k)^\dagger}^2 \right] + \mathbb{E}_{\xi_k} [\|W_{k+1} - W_k\|^2]. \end{aligned} \quad (102)$$

The proof is completed. \square

G.3. Proof of Lemma G.2: Descent of sequence W_k

Lemma G.2 (Descent Lemma of W_k). *It holds for Tiki-Taka that*

$$\begin{aligned} \|W_{k+1} - W^*\|^2 & \leq \|W_k - W^*\|^2 - \frac{\beta}{2\gamma F_{\max}} \|W_k - W^*\|_{H(W_k)}^2 \\ & \quad - \frac{\beta\gamma}{2F_{\max}} \|P^*(W_k) \odot F(W_k) - |P^*(W_k)| \odot G(W_k)\|^2 \\ & \quad + \frac{2\beta F_{\max}^3}{\gamma} \|P_{k+1} - P^*(W_k)\|_{H(W_k)^\dagger}^2 + 2\beta^2 \|P_{k+1} - P^*(W_k)\|^2. \end{aligned} \quad (73)$$

Proof of Lemma G.2. The proof begins from manipulating the norm $\|W_{k+1} - W^*\|^2$

$$\|W_{k+1} - W^*\|^2 = \|W_k - W^*\|^2 + 2 \langle W_k - W^*, W_{k+1} - W_k \rangle + \|W_{k+1} - W_k\|^2. \quad (103)$$

Revisit that we interpret P_k as an approximated solution of the constrained optimization problem (15) with W_k fixed, namely $P^*(W) := \frac{W^* - W}{\gamma}$. Therefore, we bound the second term in the RHS of (103) by

$$\begin{aligned} & 2 \langle W_k - W^*, W_{k+1} - W_k \rangle \\ & = 2 \langle W_k - W^*, \beta P_{k+1} \odot F(W_k) - \beta |P_{k+1}| \odot G(W_k) \rangle \\ & = 2\beta \langle W_k - W^*, P^*(W_k) \odot F(W_k) - |P^*(W_k)| \odot G(W_k) \rangle \\ & \quad + 2\beta \langle W_k - W^*, P_{k+1} \odot F(W_k) - |P_{k+1}| \odot G(W_k) - (P^*(W_k) \odot F(W_k) - |P^*(W_k)| \odot G(W_k)) \rangle. \end{aligned} \quad (104)$$

The first term in the RHS of (104) is bounded by

$$\begin{aligned} & 2\beta \langle W_k - W^*, P^*(W_k) \odot F(W_k) - |P^*(W_k)| \odot G(W_k) \rangle \\ & = 2\beta \left\langle (W_k - W^*) \odot \sqrt{F(W_k)}, \frac{P^*(W_k) \odot F(W_k) - |P^*(W_k)| \odot G(W_k)}{\sqrt{F(W_k)}} \right\rangle \\ & = -\frac{2\beta}{\gamma} \left\langle (W_k - W^*) \odot \sqrt{F(W_k)}, (W_k - W^*) \odot \sqrt{F(W_k)} \right\rangle \\ & \quad + \frac{2\beta}{\gamma} \left\langle (W_k - W^*) \odot \sqrt{F(W_k)}, |W_k - W^*| \odot \frac{G(W_k)}{\sqrt{F(W_k)}} \right\rangle \end{aligned} \quad (105)$$

$$\begin{aligned}
 &\stackrel{(a)}{=} -\frac{\beta}{\gamma} \|(W_k - W^*) \odot \sqrt{F(W_k)}\|^2 + \frac{\beta}{\gamma} \left\| |W_k - W^*| \odot \frac{G(W_k)}{\sqrt{F(W_k)}} \right\|^2 \\
 &\quad - \frac{\beta}{\gamma} \left\| (W_k - W^*) \odot \sqrt{F(W_k)} + |W_k - W^*| \odot \frac{G(W_k)}{\sqrt{F(W_k)}} \right\|^2 \\
 &\stackrel{(b)}{\leq} -\frac{\beta}{\gamma F_{\max}} \|W_k - W^*\|_{H(W_k)}^2 - \frac{\beta}{\gamma} \left\| (W_k - W^*) \odot \sqrt{F(W_k)} + |W_k - W^*| \odot \frac{G(W_k)}{\sqrt{F(W_k)}} \right\|^2 \\
 &\stackrel{(c)}{\leq} -\frac{\beta}{\gamma F_{\max}} \|W_k - W^*\|_{H(W_k)}^2 - \frac{\beta\gamma}{F_{\max}} \|P^*(W_k) \odot F(W_k) - |P^*(W_k)| \odot G(W_k)\|^2
 \end{aligned}$$

where (a) leverages the equality $2\langle U, V \rangle = \|U\|^2 - \|V\|^2 - \|U - V\|^2$ for any $U, V \in \mathbb{R}^D$, (b) is achieved by similar technique (62), and (c) comes from

$$\begin{aligned}
 &-\frac{\beta}{\gamma} \left\| (W_k - W^*) \odot \sqrt{F(W_k)} + |W_k - W^*| \odot \frac{G(W_k)}{\sqrt{F(W_k)}} \right\|^2 \tag{106} \\
 &= -\beta\gamma \left\| \frac{1}{\sqrt{F(W_k)}} \odot \left(\frac{W_k - W^*}{\gamma} \odot F(W_k) + \left| \frac{W_k - W^*}{\gamma} \right| \odot G(W_k) \right) \right\|^2 \\
 &\leq -\frac{\beta\gamma}{F_{\max}} \|P^*(W_k) \odot F(W_k) - |P^*(W_k)| \odot G(W_k)\|^2.
 \end{aligned}$$

The second term in the RHS of (104) is bounded by the Lipschitz continuity of analog update (c.f. Lemma C.3)

$$\begin{aligned}
 &\frac{2\beta}{\gamma} \langle W_k - W^*, P_{k+1} \odot F(W_k) - |P_{k+1}| \odot G(W_k) - (P^*(W_k) \odot F(W_k) - |P^*(W_k)| \odot G(W_k)) \rangle \\
 &\leq \frac{\beta}{2\gamma F_{\max}} \|W_k - W^*\|_{H(W_k)}^2 + \frac{2\beta F_{\max}}{\gamma} \\
 &\quad \times \|P_{k+1} \odot F(W_k) - |P_{k+1}| \odot G(W_k) - (P^*(W_k) \odot F(W_k) - |P^*(W_k)| \odot G(W_k))\|_{H(W_k)^\dagger}^2 \\
 &\leq \frac{\beta}{2\gamma F_{\max}} \|W_k - W^*\|_{H(W_k)}^2 + \frac{2\beta F_{\max}^3}{\gamma} \|P_{k+1} - P^*(W_k)\|_{H(W_k)^\dagger}^2.
 \end{aligned} \tag{107}$$

Substituting (105) and (107) into (104), we bound the second term in the RHS of (103) by

$$\begin{aligned}
 &2\langle W_k - W^*, W_{k+1} - W_k \rangle \tag{108} \\
 &\leq -\frac{\beta}{\gamma F_{\max}} \|W_k - W^*\|_{H(W_k)}^2 - \frac{\beta\gamma}{F_{\max}} \|P^*(W_k) \odot F(W_k) - |P^*(W_k)| \odot G(W_k)\|^2 \\
 &\quad + \frac{2\beta F_{\max}^3}{\gamma} \|P_{k+1} - P^*(W_k)\|_{H(W_k)^\dagger}^2.
 \end{aligned}$$

The third term in the RHS of (103) is bounded by the Lipschitz continuity of analog update (c.f. Lemma C.3)

$$\begin{aligned}
 &\|W_{k+1} - W_k\|^2 = \beta^2 \|P_{k+1} \odot F(W_k) - |P_{k+1}| \odot G(W_k)\|^2 \tag{109} \\
 &\leq 2\beta^2 \|P^*(W_k) \odot F(W_k) - |P^*(W_k)| \odot G(W_k)\|^2 \\
 &\quad + 2\beta^2 \|P_{k+1} \odot F(W_k) - |P_{k+1}| \odot G(W_k) - (P^*(W_k) \odot F(W_k) - |P^*(W_k)| \odot G(W_k))\|^2 \\
 &\leq 2\beta^2 \|P^*(W_k) \odot F(W_k) - |P^*(W_k)| \odot G(W_k)\|^2 + 2\beta^2 \|P_{k+1} - P^*(W_k)\|^2.
 \end{aligned}$$

Plugging (108) and (109) into (103) yields

$$\|W_{k+1} - W^*\|^2 \leq \|W_k - W^*\|^2 - \frac{\beta}{2\gamma F_{\max}} \|W_k - W^*\|_{H(W_k)}^2 \tag{110}$$

$$\begin{aligned}
 & - \left(\frac{\beta\gamma}{F_{\max}} - 2\beta^2 \right) \|P^*(W_k) \odot F(W_k) - |P^*(W_k)| \odot G(W_k)\|^2 \\
 & + \frac{2\beta F_{\max}^3}{\gamma} \|P_{k+1} - P^*(W_k)\|_{H(W_k)^\dagger}^2 + 2\beta^2 \|P_{k+1} - P^*(W_k)\|^2.
 \end{aligned}$$

Notice the learning rate β is chosen as $\beta \leq \frac{\gamma}{2F_{\max}}$, we have

$$\begin{aligned}
 \|W_{k+1} - W^*\|^2 & \leq \|W_k - W^*\|^2 - \frac{\beta}{2\gamma F_{\max}} \|W_k - W^*\|_{H(W_k)}^2 \\
 & - \frac{\beta\gamma}{2F_{\max}} \|P^*(W_k) \odot F(W_k) - |P^*(W_k)| \odot G(W_k)\|^2 \\
 & + \frac{2\beta F_{\max}^3}{\gamma} \|P_{k+1} - P^*(W_k)\|_{H(W_k)^\dagger}^2 + 2\beta^2 \|P_{k+1} - P^*(W_k)\|^2
 \end{aligned} \tag{111}$$

which completes the proof. \square

G.4. Proof of Lemma G.3: Descent of sequence P_k

Lemma G.3 (Descent Lemma of P_k). *Suppose Assumptions 2.2-3.3 and 4.1 hold. It holds for Tiki-Taka that*

$$\begin{aligned}
 & \mathbb{E}_{\xi_k} [\|P_{k+1} - P^*(W_k)\|^2] \\
 & \leq \left(1 - \frac{\alpha\gamma\mu L}{4(\mu + L)} \right) \|P_k - P^*(W_k)\|^2 + \frac{2\alpha(\mu + L)F_{\max}\sigma^2}{\gamma\mu L} \left\| \frac{G(P_k)}{\sqrt{F(P_k)}} \right\|_\infty^2 + \alpha^2 F_{\max}^2 \sigma^2.
 \end{aligned} \tag{81}$$

Proof of Lemma G.3. The proof begins from manipulating the norm $\|P_{k+1} - P^*(W_k)\|^2$

$$\|P_{k+1} - P^*(W_k)\|^2 = \|P_k - P^*(W_k)\|^2 + 2 \langle P_k - P^*(W_k), P_{k+1} - P_k \rangle + \|P_{k+1} - P_k\|^2. \tag{112}$$

To bound the second term, we need the following equality.

$$\begin{aligned}
 & 2\mathbb{E}_{\xi_k} [\langle P_k - P^*(W_k), P_{k+1} - P_k \rangle] \\
 & = -2\alpha \mathbb{E}_{\xi_k} [\langle P_k - P^*(W_k), \nabla f(\bar{W}_k; \xi_k) \odot F(P_k) - |\nabla f(\bar{W}_k; \xi_k)| \odot G(P_k) \rangle] \\
 & = -2\alpha \mathbb{E}_{\xi_k} [\langle P_k - P^*(W_k), \nabla f(\bar{W}_k; \xi_k) \odot F(P_k) \rangle] \\
 & \quad + 2\alpha \mathbb{E}_{\xi_k} [\langle P_k - P^*(W_k), |\nabla f(\bar{W}_k; \xi_k)| \odot G(P_k) \rangle] \\
 & = -2\alpha \langle P_k - P^*(W_k), \nabla f(\bar{W}_k) \odot F(P_k) \rangle + 2\alpha \langle P_k - P^*(W_k), |\nabla f(\bar{W}_k)| \odot G(P_k) \rangle \\
 & \quad + 2\alpha \mathbb{E}_{\xi_k} [\langle P_k - P^*(W_k), (|\nabla f(\bar{W}_k)| - |\nabla f(\bar{W}_k; \xi_k)|) \odot G(P_k) \rangle] \\
 & = -2\alpha \underbrace{\langle P_k - P^*(W_k), \nabla f(\bar{W}_k) \odot F(P_k) - |\nabla f(\bar{W}_k)| \odot G(P_k) \rangle}_{(T1)} \\
 & \quad + 2\alpha \underbrace{\mathbb{E}_{\xi_k} [\langle P_k - P^*(W_k), (|\nabla f(\bar{W}_k)| - |\nabla f(\bar{W}_k; \xi_k)|) \odot G(P_k) \rangle]}_{(T2)}
 \end{aligned} \tag{113}$$

Upper bound of the first term (T1). With Lemma C.4, the second term in the RHS of (112) can be bounded by

$$\begin{aligned}
 & -2\alpha \langle P_k - P^*(W_k), \nabla f(\bar{W}_k) \odot F(P_k) - |\nabla f(\bar{W}_k)| \odot G(P_k) \rangle \\
 & = -2\alpha \langle P_k - P^*(W_k), \nabla f(\bar{W}_k) \odot q_s(P_k) \rangle \\
 & \leq -2\alpha C_{k,+} \langle P_k - P^*(W_k), \nabla f(\bar{W}_k) \rangle + 2\alpha C_{k,-} \langle |P_k - P^*(W_k)|, |\nabla f(\bar{W}_k)| \rangle
 \end{aligned} \tag{114}$$

where $C_{k,+}$ and $C_{k,-}$ are defined by

$$C_{k,+} := \frac{1}{2} \left(\max_{i \in [D]} \{q_s([P_k]_i)\} + \min_{i \in [D]} \{q_s([P_k]_i)\} \right), \tag{115}$$

$$C_{k,-} := \frac{1}{2} \left(\max_{i \in [D]} \{q_s([P_k]_i)\} - \min_{i \in [D]} \{q_s([P_k]_i)\} \right). \quad (116)$$

In the inequality above, the first term can be bounded by the strong convexity of f . Let $\varphi(P) := f(W + \gamma P)$ which is $\gamma^2 L$ -smooth and $\gamma^2 \mu$ -strongly convex. It can be verified that $\varphi(P)$ has gradient $\nabla \varphi(P_k) = \nabla_{P_k} f(W_k + \gamma P_k) = \gamma \nabla f(\bar{W}_k)$ and optimal point $P^*(W)$. Leveraging Theorem 2.1.9 in (Nesterov, 2013), we have

$$\begin{aligned} \langle \nabla f(\bar{W}_k), P_k - P^*(W_k) \rangle &= \frac{1}{\gamma} \langle \nabla \varphi(P_k), P_k - P^*(W_k) \rangle \\ &\geq \frac{1}{\gamma} \left(\frac{\gamma^2 \mu \cdot \gamma^2 L}{\gamma^2 \mu + \gamma^2 L} \|P_k - P^*(W_k)\|^2 + \frac{1}{\gamma^2 \mu + \gamma^2 L} \|\nabla \varphi(P_k)\|^2 \right) \\ &= \frac{\gamma \mu L}{\mu + L} \|P_k - P^*(W_k)\|^2 + \frac{1}{\gamma(\mu + L)} \|\nabla f(\bar{W}_k)\|^2. \end{aligned} \quad (117)$$

The second term in the RHS of (114) can be bounded by Young's inequality $2 \langle x, y \rangle \leq u \|x\|^2 + \frac{1}{u} \|y\|^2$ with any $u > 0$ and $x, y \in \mathbb{R}^D$

$$\begin{aligned} &2\alpha C_{k,-} \langle |P_k - P^*(W_k)|, |\nabla f(\bar{W}_k)| \rangle \\ &\leq \frac{\alpha C_{k,-}^2 - \gamma(\mu + L)}{C_{k,+}} \|P_k - P^*(W_k)\|^2 + \frac{\alpha C_{k,+}}{\gamma(\mu + L)} \|\nabla f(\bar{W}_k)\|^2 \end{aligned} \quad (118)$$

where u is chosen to align the coefficient in front of $\|\nabla f(\bar{W}_k)\|^2$. Therefore, (T1) in (114) becomes

$$\begin{aligned} &-2\alpha \langle P_k - P^*(W_k), \nabla f(\bar{W}_k) \odot F(P_k) - |\nabla f(\bar{W}_k)| \odot G(P_k) \rangle \\ &\leq - \left(\frac{2\alpha \gamma \mu L C_{k,+}}{\mu + L} - \frac{\alpha C_{k,-}^2 - \gamma(\mu + L)}{C_{k,+}} \right) \|P_k - P^*(W_k)\|^2 - \frac{\alpha C_{k,+}}{\gamma(\mu + L)} \|\nabla f(\bar{W}_k)\|^2. \end{aligned} \quad (119)$$

Upper bound of the second term (T2). Leveraging the Young's inequality $2 \langle x, y \rangle \leq u \|x\|^2 + \frac{1}{u} \|y\|^2$ with any $u > 0$ and $x, y \in \mathbb{R}^D$, we have

$$\begin{aligned} &2\alpha \mathbb{E}_{\xi_k} [\langle P_k - P^*(W_k), (|\nabla f(\bar{W}_k)| - |\nabla f(\bar{W}_k; \xi_k)|) \odot G(P_k) \rangle] \\ &= 2\alpha \mathbb{E}_{\xi_k} \left[\left\langle (P_k - P^*(W_k)) \odot \sqrt{F(P_k)}, (|\nabla f(\bar{W}_k)| - |\nabla f(\bar{W}_k; \xi_k)|) \odot \frac{G(P_k)}{\sqrt{F(P_k)}} \right\rangle \right] \\ &\stackrel{(a)}{\leq} \frac{\alpha \gamma \mu L C_{k,+}}{(\mu + L) F_{\max}} \|(P_k - P^*(W_k)) \odot \sqrt{F(P_k)}\|^2 \\ &\quad + \frac{\alpha(\mu + L) F_{\max}}{\gamma \mu L C_{k,+}} \mathbb{E}_{\xi_k} \left[\left\| (|\nabla f(\bar{W}_k)| - |\nabla f(\bar{W}_k; \xi_k)|) \odot \frac{G(P_k)}{\sqrt{F(P_k)}} \right\|^2 \right] \\ &\stackrel{(b)}{\leq} \frac{\alpha \gamma \mu L C_{k,+}}{(\mu + L) F_{\max}} \|(P_k - P^*(W_k)) \odot \sqrt{F(P_k)}\|^2 \\ &\quad + \frac{\alpha(\mu + L) F_{\max}}{\gamma \mu L C_{k,+}} \mathbb{E}_{\xi_k} \left[\left\| (|\nabla f(\bar{W}_k)| - |\nabla f(\bar{W}_k; \xi_k)|) \odot \frac{G(P_k)}{\sqrt{F(P_k)}} \right\|^2 \right] \\ &\stackrel{(c)}{=} \frac{\alpha \gamma \mu L C_{k,+}}{(\mu + L) F_{\max}} \|(P_k - P^*(W_k)) \odot \sqrt{F(P_k)}\|^2 + \frac{\alpha(\mu + L) F_{\max} \sigma^2}{\gamma \mu L C_{k,+}} \left\| \frac{G(P_k)}{\sqrt{F(P_k)}} \right\|_{\infty}^2 \\ &\stackrel{(d)}{\leq} \frac{\alpha \gamma \mu L C_{k,+}}{\mu + L} \|P_k - P^*(W_k)\|^2 + \frac{\alpha(\mu + L) F_{\max} \sigma^2}{\gamma \mu L C_{k,+}} \left\| \frac{G(P_k)}{\sqrt{F(P_k)}} \right\|_{\infty}^2 \end{aligned} \quad (120)$$

where (a) choose $u > 0$ to align the coefficient in front of $\|(P_k - P^*(W_k)) \odot \sqrt{F(P_k)}\|^2$ in the RHS of (119), (b) applies $\|x\| - \|y\| \leq \|x - y\|$ for any $x, y \in \mathbb{R}$, (c) uses the bounded variance assumption (c.f. Assumption 3.3), and (d) leverages the fact that $F(P_k)$ is bounded by F_{\max} element-wise.

Combining the upper bound of (T1) and (T2), we bound (113) by

$$\begin{aligned}
 & 2\mathbb{E}_{\xi_k}[\langle P_k - P^*(W_k), P_{k+1} - P_k \rangle] \\
 & \leq - \left(\frac{\alpha\gamma\mu LC_{k,+}}{\mu + L} - \frac{\alpha C_{k,-}^2 \gamma(\mu + L)}{C_{k,+}} \right) \|P_k - P^*(W_k)\|^2 \\
 & \quad - \frac{\alpha C_{k,+}}{\gamma(\mu + L)} \|\nabla f(\bar{W}_k)\|^2 + \frac{\alpha(\mu + L)F_{\max}\sigma^2}{\gamma\mu LC_{k,+}} \left\| \frac{G(P_k)}{\sqrt{F(P_k)}} \right\|_{\infty}^2 \\
 & \leq - \frac{\alpha\gamma\mu LC_{k,+}}{2(\mu + L)} \|P_k - P^*(W_k)\|^2 - \frac{\alpha C_{k,+}}{\gamma(\mu + L)} \|\nabla f(\bar{W}_k)\|^2 + \frac{\alpha(\mu + L)F_{\max}\sigma^2}{\gamma\mu LC_{k,+}} \left\| \frac{G(P_k)}{\sqrt{F(P_k)}} \right\|_{\infty}^2
 \end{aligned} \tag{121}$$

where the last inequality holds when γ is sufficiently large, P_k as well as $C_{k,-}$ are sufficiently closed to 0, and the following inequality holds

$$(\mu + L) \frac{C_{k,-}^2}{C_{k,+}^2} \leq \frac{\mu L}{2(\mu + L)}. \tag{122}$$

Furthermore, the last term in the RHS of (112) can be bounded by the Lipschitz continuity of analog update (c.f. Lemma C.3) and the bounded variance assumption (c.f. Assumption 3.3)

$$\begin{aligned}
 \mathbb{E}_{\xi_k}[\|P_{k+1} - P_k\|^2] & = \mathbb{E}_{\xi_k}[\|\alpha\nabla f(\bar{W}_k; \xi_k) \odot F(P_k) - \alpha|\nabla f(\bar{W}_k; \xi_k)| \odot G(P_k)\|^2] \\
 & \leq \alpha^2 F_{\max}^2 \mathbb{E}_{\xi_k}[\|\nabla f(\bar{W}_k; \xi_k)\|^2] \\
 & = \alpha^2 F_{\max}^2 \|\nabla f(\bar{W}_k)\|^2 + \alpha^2 F_{\max}^2 \sigma^2 \\
 & \leq \frac{\alpha C_{k,+}}{\gamma(\mu + L)} \|\nabla f(\bar{W}_k)\|^2 + \alpha^2 F_{\max}^2 \sigma^2
 \end{aligned} \tag{123}$$

where the last inequality holds if α is sufficiently small.

Plugging inequality (121) and (123) above into (112) yields

$$\begin{aligned}
 & \mathbb{E}_{\xi_k}[\|P_{k+1} - P^*(W_k)\|^2] \\
 & \leq \left(1 - \frac{\alpha\gamma\mu LC_{k,+}}{2(\mu + L)} \right) \|P_k - P^*(W_k)\|^2 + \frac{\alpha(\mu + L)F_{\max}\sigma^2}{\gamma\mu LC_{k,+}} \left\| \frac{G(P_k)}{\sqrt{F(P_k)}} \right\|_{\infty}^2 + \alpha^2 F_{\max}^2 \sigma^2.
 \end{aligned} \tag{124}$$

By definition of $C_{k,+}$, when the saturation degree of P_k is properly limited, we have $C_{k,+} \geq \frac{1}{2}$. Therefore, we have

$$\begin{aligned}
 & \mathbb{E}_{\xi_k}[\|P_{k+1} - P^*(W_k)\|^2] \\
 & \leq \left(1 - \frac{\alpha\gamma\mu L}{4(\mu + L)} \right) \|P_k - P^*(W_k)\|^2 + \frac{2\alpha(\mu + L)F_{\max}\sigma^2}{\gamma\mu L} \left\| \frac{G(P_k)}{\sqrt{F(P_k)}} \right\|_{\infty}^2 + \alpha^2 F_{\max}^2 \sigma^2
 \end{aligned} \tag{125}$$

which completes the proof. \square

G.5. Proof of Corollary 4.4: Exact convergence of Tiki-Taka

Corollary 4.4 (Exact convergence of Tiki-Taka). *Under Assumption 4.3 and the conditions in Theorem 4.2, if $\gamma \geq \Omega(H_{\min}^{-1/5})$, it holds that $E_K^{\text{TT}} \leq O(\sqrt{\sigma^2 L/K})$.*

Proof of Corollary 4.4. From Theorem 4.2, we have

$$\|\nabla f(\bar{W}_k)\|^2 \leq O(E_K^{\text{TT}}) \leq O\left(F_{\max}^2 \sqrt{\frac{(f(W_0) - f^*)\sigma^2 L}{K}}\right) + 24F_{\max}\sigma^2 S_K^{\text{TT}}. \tag{126}$$

Under the zero-shift assumption (Assumption 4.3) and the Lipschitz continuity of the response functions, it holds directly that

$$\left\| \frac{G(P_k)}{\sqrt{F(P_k)}} \right\|_{\infty}^2 \leq \left\| \frac{G(P_k)}{\sqrt{F(P_k)}} \right\|^2 = \left\| \frac{G(P_k)}{\sqrt{F(P_k)}} - \frac{G(0)}{\sqrt{F(0)}} \right\|^2 \leq L_S^2 \|P_k\|^2 \quad (127)$$

where $L_S \geq 0$ is a constant. Using $\|U + V\|^2 \leq 2\|U\|^2 + 2\|V\|^2$ for any $U, V \in \mathbb{R}^D$, we have

$$\|P_k\|^2 \leq 2\|P_k - P^*(W_k)\|^2 + 2\|P^*(W_k)\|^2 = 2\|P_k - P^*(W_k)\|^2 + \frac{2}{\gamma^2} \|W_k - W^*\|^2 \quad (128)$$

where the last inequality comes from the definition of $P^*(W_k)$, as well as the definition of $P^*(W)$. Recall that convergence metric E_K^{TT} defined in (87) is in the order of

$$\begin{aligned} E_K^{\text{TT}} &\geq \Omega \left(\gamma^3 \|W_k - W^*\|_{H(W_k)}^2 + \gamma^2 \|P_k - P^*(W_k)\|^2 \right) \\ &\geq \Omega \left(\min\{H(W_k)\} \gamma^3 \|W_k - W^*\|^2 + \gamma^2 \|P_k - P^*(W_k)\|^2 \right) \\ &\geq \Omega \left(\frac{1}{\gamma^2} \|W_k - W^*\|^2 + \gamma^2 \|P_k - P^*(W_k)\|^2 \right). \end{aligned} \quad (129)$$

Therefore, we have

$$S_K^{\text{TT}} = \frac{1}{K} \sum_{k=0}^K \left\| \frac{G(P_k)}{\sqrt{F(P_k)}} \right\|_{\infty}^2 \leq \frac{1}{K} \sum_{k=0}^K \left(2\|P_k - P^*(W_k)\|^2 + \frac{2}{\gamma^2} \|W_k - W^*\|^2 \right) \leq O(E_K^{\text{TT}}) \quad (130)$$

where the last inequality holds if γ is sufficiently large. Considering that, $E_K^{\text{TT}} - S_K^{\text{TT}} \geq \overline{O}(E_K^{\text{TT}}) \geq 0$ and the conclusion is reached directly from Theorem 4.2. \square

H. Proof of Theorem H.1: Convergence of Analog GD

In Section 3.2, we showed that Analog SGD converges to a critical point inexactly with asymptotic error proportional to the noise variance σ^2 . Intuitively, without the effect of noise, Analog GD converges to the critical point. Define the convergence metric by

$$E_K^{\text{AGD}} := \frac{1}{K} \sum_{k=0}^{K-1} \left(\|\nabla f(W_k) \odot F(W_k) - |\nabla f(W_k)| \odot G(W_k)\|^2 + \|\nabla f(W_k)\|_{H(W_k)}^2 \right). \quad (131)$$

The convergence is guaranteed by the following theorem.

Theorem H.1 (Convergence of Analog GD). *Under Assumption 3.2–3.3, it holds that*

$$E_K^{\text{AGD}} \leq \frac{8L(f(W_0) - f^*)F_{\max}^2}{K}. \quad (132)$$

Further, if $H_{\min}^{\text{ASGD}} := \min_{k \in [K]} \min\{Q_+(W_k)Q_-(W_k)\} > 0$, it holds that

$$\frac{1}{K} \sum_{k=0}^{K-1} \|\nabla f(W_k)\|^2 \leq \frac{2L(f(W_0) - f^*)F_{\max}^2}{KH_{\min}^{\text{ASGD}}}. \quad (133)$$

Proof of Theorem H.1. The L -smooth assumption (Assumption 3.2) implies that

$$\begin{aligned} f(W_{k+1}) &\leq f(W_k) + \langle \nabla f(W_k), W_{k+1} - W_k \rangle + \frac{L}{2} \|W_{k+1} - W_k\|^2 \\ &= f(W_k) - \frac{\alpha}{2} \|\nabla f(W_k) \odot \sqrt{F(W_k)}\|^2 - \frac{1}{F_{\max}} \left(\frac{1}{2\alpha} - \frac{LF_{\max}}{2} \right) \|W_{k+1} - W_k\|^2 \end{aligned} \quad (134)$$

$$+ \frac{1}{2\alpha} \left\| \frac{W_{k+1} - W_k}{\sqrt{F(W_k)}} + \alpha \nabla f(W_k) \odot \sqrt{F(W_k)} \right\|^2$$

where the second inequality comes from

$$\begin{aligned} \langle \nabla f(W_k), W_{k+1} - W_k \rangle &= \alpha \left\langle \nabla f(W_k) \odot \sqrt{F(W_k)}, \frac{W_{k+1} - W_k}{\alpha \sqrt{F(W_k)}} \right\rangle \\ &= -\frac{\alpha}{2} \|\nabla f(W_k) \odot \sqrt{F(W_k)}\|^2 - \frac{1}{2\alpha} \left\| \frac{W_{k+1} - W_k}{\sqrt{F(W_k)}} \right\|^2 \\ &\quad + \frac{1}{2\alpha} \left\| \frac{W_{k+1} - W_k}{\sqrt{F(W_k)}} + \alpha \nabla f(W_k) \odot \sqrt{F(W_k)} \right\|^2 \end{aligned} \quad (135)$$

as well as the inequality

$$\left\| \frac{W_{k+1} - W_k}{\sqrt{F(W_k)}} \right\|^2 \geq \frac{1}{F_{\max}} \|W_{k+1} - W_k\|^2. \quad (136)$$

The third term in the RHS of (134) can be bounded by

$$\frac{1}{2\alpha} \left\| \frac{W_{k+1} - W_k}{\sqrt{F(W_k)}} + \alpha \nabla f(W_k) \odot \sqrt{F(W_k)} \right\|^2 = \frac{\alpha}{2} \left\| |\nabla f(W_k)| \odot \frac{G(W_k)}{\sqrt{F(W_k)}} \right\|^2. \quad (137)$$

Define the saturation vector $H(W_k) \in \mathbb{R}^D$ by

$$\begin{aligned} H(W_k) &:= F(W_k)^{\odot 2} - G(W_k)^{\odot 2} = (F(W_k) + G(W_k)) \odot (F(W_k) - G(W_k)) \\ &= q_+(W_k) \odot q_-(W_k). \end{aligned} \quad (138)$$

Notice the following inequality is valid

$$\begin{aligned} &-\frac{\alpha}{2} \|\nabla f(W_k) \odot \sqrt{F(W_k)}\|^2 + \frac{\alpha}{2} \left\| |\nabla f(W_k)| \odot \frac{G(W_k)}{\sqrt{F(W_k)}} \right\|^2 \\ &= -\frac{\alpha}{2} \sum_{d \in [D]} \left([\nabla f(W_k)]_d^2 \left([F(W_k)]_d - \frac{[G(W_k)]_d^2}{[F(W_k)]_d} \right) \right) \\ &= -\frac{\alpha}{2} \sum_{d \in [D]} \left([\nabla f(W_k)]_d^2 \left(\frac{[F(W_k)]_d^2 - [G(W_k)]_d^2}{[F(W_k)]_d} \right) \right) \\ &\leq -\frac{\alpha}{2F_{\max}} \sum_{d \in [D]} \left([\nabla f(W_k)]_d^2 ([F(W_k)]_d^2 - [G(W_k)]_d^2) \right) \\ &= -\frac{\alpha}{2F_{\max}} \|\nabla f(W_k)\|_{S_k}^2 \leq 0. \end{aligned} \quad (139)$$

Substituting (137) and (139) back into (134) yields

$$\frac{1}{F_{\max}} \left(\frac{1}{2\alpha} - \frac{LF_{\max}}{2} \right) \|W_{k+1} - W_k\|^2 \leq f(W_k) - f(W_{k+1}). \quad (140)$$

Noticing that $\|W_{k+1} - W_k\|^2 = \alpha^2 \|\nabla f(W_k) \odot F(W_k) - |\nabla f(W_k)| \odot G(W_k)\|^2$ and averaging for k from 0 to $K-1$, we have

$$E_K^{\text{AGD}} = \frac{1}{K} \sum_{k=0}^{K-1} \left(\|\nabla f(W_k) \odot F(W_k) - |\nabla f(W_k)| \odot G(W_k)\|^2 + \|\nabla f(W_k)\|_{H(W_k)}^2 \right) \quad (141)$$

$$\leq \frac{2(f(W_0) - f(W_{K+1}))F_{\max}}{\alpha(1 - \alpha LF_{\max})K} \leq \frac{8L(f(W_0) - f^*)F_{\max}^2}{K}$$

where the last inequality choose $\alpha = \frac{1}{2LF_{\max}}$.

Further, if the degree of saturation is bounded, (134)–(139) implies that

$$\frac{\alpha H_{\min}^{\text{AGD}}}{2} \|\nabla f(W_k)\|^2 \leq \frac{\alpha}{2} \|\nabla f(W_k)\|_{H(W_k)}^2 \leq f(W_k) - f(W_{k+1}). \quad (142)$$

Averaging (142) for k from 0 to K deduce that

$$\frac{1}{K} \sum_{k=0}^{K-1} \|\nabla f(W_k)\|^2 \leq \frac{2(f(W_0) - f(W_{K+1}))F_{\max}}{\alpha K H_{\min}^{\text{AGD}}} \leq \frac{2L(f(W_0) - f^*)F_{\max}^2}{K H_{\min}^{\text{AGD}}} \quad (143)$$

where the second inequality holds because the learning rate is selected as $\alpha = \frac{1}{LF_{\max}}$. \square

I. Simulation Details and Additional Results

This section provides details about the experiments in Section 5. All simulation is performed under the PYTORCH framework <https://github.com/pytorch/pytorch>. The analog training algorithms, including Analog SGD and Tiki-Taka, are provided by the open-source simulation toolkit AIHWKIT (Rasch et al., 2021), which has MIT license; see github.com/IBM/aihwkit.

Optimizer. The digital SGD optimizer is implemented by `FloatingPointRPUConfig` in AIHWKIT, which is equivalent to the SGD implemented in PYTORCH. The Analog SGD is implemented by selecting `SingleRPUConfig` as configuration, and Tiki-Taka optimizers are implemented by `UnitCellRPUConfig` with `TransferCompound` devices in AIHWKIT.

Hardware. We conduct our experiments on one NVIDIA RTX 3090 GPU, which has 24GB memory and a maximum power of 350W. The simulations take from 30 minutes to 5 hours, depending on model sizes and datasets.

Statistical Significance. The simulation data reported in all tables is repeated three times. The randomness originates from the data shuffling, random initialization, and random noise in the analog hardware. The mean and standard deviation are calculated using *statistics* library.

I.1. Power and Exponential Response Functions

The *power response* is a power function, given by

$$q_+(w) = \left(1 - \frac{w}{\tau}\right)^{\gamma_{\text{res}}}, \quad q_-(w) = \left(1 + \frac{w}{\tau}\right)^{\gamma_{\text{res}}} \quad (144)$$

which can be changed by adjusting the dynamic radius τ and shape parameter γ_{res} . We also consider the *exponential response*, whose response is an exponential function, defined by

$$q_+(w) = \frac{\exp(\gamma_{\text{res}}(1 - w/\tau)) - 1}{\exp(\gamma_{\text{res}}) - 1}, \quad q_-(w) = \frac{\exp(\gamma_{\text{res}}(1 + w/\tau)) - 1}{\exp(\gamma_{\text{res}}) - 1}. \quad (145)$$

It could be checked that the boundary of their dynamic ranges are $\tau^{\max} = \tau$ and $\tau^{\min} = -\tau$, while the symmetric point is 0, as required by Corollary 4.4. Figure 5 illustrates how the response functions change with different γ_{res} .

I.2. Least squares problem

In Figure 2 (see Section 1.2), we consider the least squares problem on a synthetic dataset and a ground truth $W^* \in \mathbb{R}^D$. The problem can be formulated by

$$\min_{W \in \mathbb{R}^D} f(W) := \frac{1}{2} \|AW - b\|^2 = \frac{1}{2} \|A(W - W^*)\|^2. \quad (146)$$

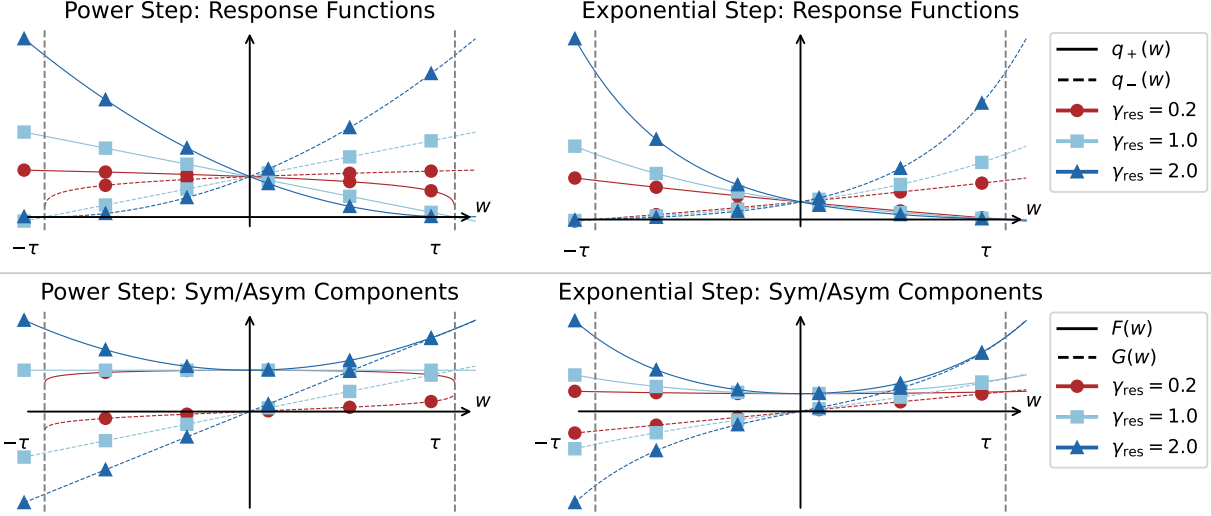


Figure 5: Examples of response functions. The dependence of the response function on the weight w can grow at various rates, including but not limited to power (Left) or exponential rate (Right). τ is the radius of the dynamic range, and γ_{res} is a parameter that needs to be determined by physical measurements.

The elements of W^* are sampled from a Gaussian distribution with mean 0 and variance $\sigma_{W^*}^2$. Consider a matrix $A \in \mathbb{R}^{D_{out} \times D}$ of size $D = 50$ and $D_{out} = 100$ whose elements are sampled from a Gaussian distribution with variance σ_A^2 . The label $b \in \mathbb{R}^{D_{out}}$ is generated by $b = AW^*$ where W^* are sampled from a standard Gaussian distribution with $\sigma_{W^*}^2$. The response granularity $\Delta w_{min} = 1e-4$ while $\tau = 3.5$. The maximum bit length is 8. The variance are set as $\sigma_A^2 = 1.00^2$, $\sigma_{W^*}^2 = 0.5^2$.

I.3. Classification problem

We conduct training simulations of image classification tasks on a series of real datasets. In the implementation of Tiki-Taka, only a few columns or rows of P_k are transferred per time to W_k in the recursion (17) to balance the communication and computation. In our simulations, we transfer 1 column every time. The response granularity is set as $\Delta w_{min} = 1e-3$.

The other setting follows the settings of AIHWKIT, including output noise (0.5 % of the quantization bin width), quantization and clipping (output range set 20, output noise 0.1, and input and output quantization to 8 bits). Noise and bound management techniques are used in (Gokmen et al., 2017). A learnable scaling factor is set after each analog layer, which is updated using SGD.

3-FC / MNIST. Following the setting in (Gokmen & Vlasov, 2016), we train a model with 3 fully connected layers. The hidden sizes are 256 and 128. The activation functions are Sigmoid. The learning rates are $\alpha = 0.1$ for Digital SGD, $\alpha = 0.05, \beta = 0.01$ for Analog SGD and Tiki-Taka. The batch size is 10 for all algorithms.

CNN / MNIST. We train a convolution neural network, which contains 2-convolutional layers, 2-max-pooling layers, and 2-fully connected layers. The activation functions are Tanh. The first two convolutional layers use 5×5 kernels with 16 and 32 kernels, respectively. Each convolutional layer is followed by a subsampling layer implemented by the max pooling function over non-overlapping pooling windows of size 2×2 . The output of the second pooling layer, consisting of 512 neuron activations, feeds into a fully connected layer consisting of 128 tanh neurons, which is then connected into a 10-way softmax output layer. The learning rates are set as $\alpha = 0.1$ for Digital SGD, $\alpha = 0.05, \beta = 0.01$ for Analog SGD or Tiki-Taka. The batch size is 8 for all algorithms.

ResNet / CIFAR10 & CIFAR100. We train different models from the ResNet family, including ResNet18, 34, and 50. The base model is pre-trained on ImageNet dataset. The last fully connected layer is replaced by an analog layer. The learning rates are set as $\alpha = 0.075$ for Digital SGD, $\alpha = 0.075, \beta = 0.01$ for Analog SGD or Tiki-Taka.

Tiki-Taka adopts $\gamma = 0.4$ unless stated otherwise. The batch size is 128 for all algorithms. Power response with $\gamma_{\text{res}} = 3.0$ and $\tau = 0.1$, and exponential response with $\gamma_{\text{res}} = 3.0$ and $\tau = 0.1$, are used in the simulations.

I.4. Additional performance on real datasets

We train different models from the MobileNet family, including MobileNet2, MobileNetV3L, MobileNetV3S. The base model is pre-trained on ImageNet dataset. The last fully connected layer is replaced by an analog layer. The learning rates are set as $\alpha = 0.075$ for Digital SGD, $\alpha = 0.075, \beta = 0.01$ for Analog SGD or Tiki-Taka. Tiki-Taka adopts $\gamma = 0.4$ unless stated otherwise. The batch size is 128 for all algorithms. Power response function with $\gamma_{\text{res}} = 4.0$ and $\tau = 0.05$ is used in the simulations.

CIFAR10/CIFAR100 ResNet. We fine-tune three models from the ResNet family with different scales on CIFAR10/CIFAR100 datasets. The power response functions with the parameter $\gamma_{\text{res}} = 3.0$ and $\tau = 0.1$ is used, whose results are shown in Table 1 and 3, respectively. The results show that the Tiki-Taka outperforms Analog SGD by about 1.0% in most of the cases in ResNet34/50, and the gap even reaches about 10.0% for ResNet18 training on the CIFAR100 dataset. An interesting observation is that the gap is closer on the exponential response, at which time Analog SGD achieves a comparable and sometimes higher accuracy with Tiki-Taka. We speculate it happens because the asymmetric bias, coupled with the impact of a high-dimensional objective landscape, leads to a better local minimum, which is worthy of study in future work.

	CIFAR10			CIFAR100		
	DSGD	ASGD	TT	DSGD	ASGD	TT
ResNet18	95.43±0.13	94.66±0.11	94.70±0.07	81.12±0.25	73.55±0.22	74.64±0.24
ResNet34	96.48±0.02	96.19±0.04	96.24±0.08	83.86±0.12	78.10±0.24	79.05±0.21
ResNet50	96.57±0.10	96.53±0.06	96.40±0.13	83.98±0.11	81.40±0.36	79.75±0.10

Table 3: Analog training with the *exponential response* for fine-tuning task on CIFAR10/100 datasets using models from ResNet family. The accuracy of the test set is reported. DSGD, ASGD, and TT represent Digital SGD, Analog SGD, Tiki-Taka, respectively.

CIFAR10/CIFAR100 MobileNet. We fine-tune three models from the MobileNet family with different scales on CIFAR10/CIFAR100 datasets. The response function are set as the power response with the parameter $\gamma_{\text{res}} = 4.0$ and $\tau = 0.05$, whose results are shown in Table 4. In the simulations, the accuracy of Analog SGD drops significantly by about 10% in most cases, while Tiki-Taka remains comparable to the Digital SGD with only a slight drop.

I.5. Ablation study on cycle variation

To verify the conclusion of Theorem 2.1 that the error introduced by cycle variation is a higher-order term, we conduct a numerical simulation training on image classification task on MNIST dataset using Fully-connected network (FCN) or convolution neural network (CNN) network. In the pulse update (2), the parameter σ_c is varied from 10% to 120%, where the noise signal is already larger than the response function signal itself. The results are shown in Table 5. The results show that the test accuracy of both Analog SGD and Tiki-Taka is not significantly affected by the cycle variation, which complies with the theoretical analysis.

	CIFAR10			CIFAR100		
	DSGD	ASGD	TT	DSGD	ASGD	TT
MobileNetV2	95.28±0.20	94.34±0.27	95.05±0.11	80.60±0.18	63.41±1.20	73.33±0.94
MobileNetV3S	94.45±0.10	80.66±6.18	93.65±0.24	78.94±0.05	51.79±1.05	71.14±0.93
MobileNetV3L	95.95±0.08	80.79±2.97	95.39±0.27	82.16±0.26	66.80±1.40	78.81±0.52

Table 4: Analog training with exponential response for fine-tuning task on CIFAR10/100 datasets using models from the MobileNet family. The accuracy of the test set is reported. DSGD, ASGD, and TT represent Digital SGD, Analog SGD, Tiki-Taka, respectively.

	FCN			CNN		
	DSGD	ASGD	TT	DSGD	ASGD	TT
$\sigma_c = 10\%$	98.17±0.05	97.22±0.21	97.66±0.04	99.09±0.04	92.68±0.45	98.74±0.07
$\sigma_c = 30\%$		96.97±0.12	97.07±0.12		93.36±0.55	98.89±0.05
$\sigma_c = 60\%$		96.33±0.21	97.70±0.09		93.07±0.53	98.68±0.09
$\sigma_c = 90\%$		95.99±0.15	97.44±0.15		91.87±0.48	98.92±0.02
$\sigma_c = 120\%$		96.19±0.20	96.97±0.20		91.57±0.58	98.85±0.04

Table 5: Test accuracy comparison under different cycle variation levels σ_c on MNIST dataset. DSGD, ASGD, and TT represent Digital SGD, Analog SGD, Tiki-Taka, respectively

I.6. Ablation study on various response functions

We also train a FCN model on the MNIST dataset under various response functions. As shown in the figure, larger γ_{res} leads to a steeper response function. The results are shown in Table 6. The accuracy < 15.00 in the table implies that Analog SGD fails completely at all trials, which is close to random guess. The results show that Analog SGD works well only when the asymmetric is mild, i.e. γ_{res} is small and τ is large, while Tiki-Taka outperforms Analog SGD and achieves comparable accuracy with Digital SGD.

		DSGD	Power response		Exponential response	
			ASGD	TT	ASGD	TT
$\gamma_{res} = 0.5$	$\tau = 0.6$	98.17±0.05	96.01±0.26	96.92±0.19	<15.00	97.27±0.07
	$\tau = 0.7$		97.40±0.15	97.05±0.05	<15.00	97.39±0.15
	$\tau = 0.8$		97.38±0.10	96.82±0.17	94.00±0.63	97.16±0.16
$\gamma_{res} = 1.0$	$\tau = 0.6$		<15.00	97.39±0.05	<15.00	97.46±0.08
	$\tau = 0.7$		<15.00	97.33±0.05	<15.00	97.49±0.04
	$\tau = 0.8$		<15.00	97.34±0.09	<15.00	97.25±0.16
$\gamma_{res} = 2.0$	$\tau = 0.6$		<15.00	96.93±0.15	<15.00	97.19±0.16
	$\tau = 0.7$		<15.00	97.27±0.02	<15.00	97.72±0.07
	$\tau = 0.8$		<15.00	97.18±0.04	<15.00	97.06±0.10

Table 6: Test accuracy comparison under different response function parameters τ and γ_{res} for FCN training on MNIST dataset with power or exponential response functions. DSGD, ASGD, and TT represent Digital SGD, Analog SGD, Tiki-Taka, respectively.

I.7. Ablation study on γ

We conduct a series of simulations to study the impact of mixing coefficient γ in (16) on CIFAR10 or CIFAR100 dataset in the ResNet training tasks. The results are presented in Figure 6, which shows that Tiki-Taka achieves a great accuracy gain from increasing γ from 0 to 0.1, while the gain saturates after that. Therefore, we conclude that Tiki-Taka benefits from a non-zero γ , and the performance is robust to the γ selection.

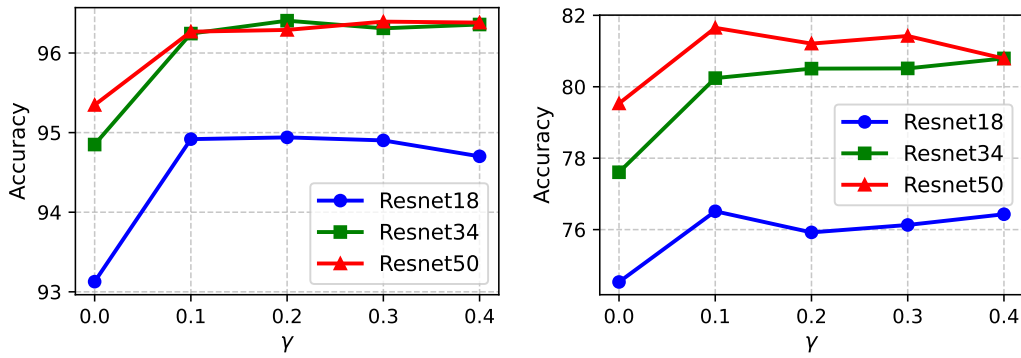


Figure 6: The test accuracy of ResNet family models after 100 epochs trained by Tiki-Taka under different γ in (16); (Left) CIFAR10. (Right) CIFAR100.